AD __409 062__

DEFENSE DOCUMENTATION CENTER
FOR

SCIENTIFIC AND TECHNICAL INFORMATION

CAMERON STATION. ALEXANDRIA. VIRGINIA

FTD-TT· 62-1288

N- 63-4-2

409 062

TRANSLATION

METALLURGY AND METALLOGRAPHY OF PURE METALS
(SELECTED ARTICLES)

FOREIGN TECHNOLOGY

DIVISION

AIR FORCE SYSTEMS COMMAND

WRIGHT-PATTERSON AIR FORCE BASE

OHIO
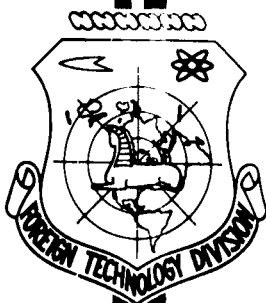
UNEDITED ROUGH DRAFT TRANSLATION

METALLURGY AND METALLOGRAPHY OF PURE METALS (SELECTED ARTICLES)

English Pages: 67

SOURCE: Russian Book, Metallurgiya i Metallovedeniye
Chistykh Metallov, Sbornik Nauchnykh Rabot Pod
Redaktsiye, Gosatomizdat, Moskva, Vol. 3, 1961,
pp. 64-73, 152-162, 175-182, 190-192, 233-248,
284-289

TABLE OF CONTENTS

- 1 -

INVESTIGATION OF THE OXIDATION,KINETICS OF IODIDE HAFNIUM

IN THE TEMPERATURE RANGE FROM 600 TO 1000°C

A. I. Yevstyukhin, I. I. Korobkov and I. P. Barinov

INTRODUCTION

The present work is devoted to study of the oxidation kinetics of iodide hafnium in oxygen at temperatures within the range from 600 to 1000°C. Interest is drawn to this problem firstly by the use of hafnium in a number of new engineering fields and secondly by the fact that the combination of the properties of the metallic base and oxide film which forms on the surface of hafnium on heating to high temperatures is exceptionally good with this metal.

As we know, hafnium oxide (HfO_2) is an extremely high-melting compound. Its melting point is nearly 800°C above that of metallic hafnium and is approximately 2800°C [1]. It does not undergo polymorphic transformations below 1700°C. The high value of the heat of formation of this compound (approximately 266 kilocalories/mole) indicates its high thermal and chemical stability.

Only one work [2] devoted to investigation of the oxidation kinetics of hafnium within the temperature range from 350 to 1200°C has been published in the literature. The authors of this work note that in the oxidation process of hafnium, an extremely strong and compact oxide film with high protective properties forms on its surface.

According to the authors of [2], the oxidation kinetics of hafnium may be characterized, in general, by logarithmic and parabolic curves. Under certain conditions, however, the parabolic oxidation

- 1 -

curve of hafnium transforms into a linear curve. This is observed when a porous white oxide forms over the compact oxide layer (which increases only to a certain thickness).

In the opinion of the authors of [2], the porous layer of hafnium oxide forms at a thickness of the compact oxide film such that the [compressive] stresses in the latter reach a magnitude which gives rise to cracking in the oxide film.

The authors of [2] also established that the dependence of the oxidation rate constant of hafnium upon temperature is clearly expressed by the Arrhenius relationship. Proceeding from this, they computed the values of the activation energy of the oxidation process individually for the logarithmic, parabolic and linear oxidation curves, which were found to be 11.4, 36.0 and 26.1 kcal/mole, respectively. These investigators did not detect variations in the oxidation rate constants with oxygen pressure (from 10 to 760 mm Hg).

The structure of the oxide films which form on hafnium were also studied in [2]. According to x-ray data, the film of hafnium oxide on the metal has a monoclinic lattice.

In regard to the oxidation mechanism of hafnium, the authors of [2] consider that the oxidation of hafnium proceeds by the diffusion of oxygen ions through the anion vacancies in the oxide and by subsequent reaction with the hafnium on the metal-oxide boundary.

Evaluating [2] as a whole, it is necessary to note that the data obtained in it did not refer to pure hafnium, but to its alloy with 5% of zirconium, since the initial hafnium contained a considerable quantity of impurities (including 5% Zr, 0.02% Fe and others).

In our investigation, we used hafnium with a low zirconium content (less than 1%). The hafnium that we used was purified of nonmetallic and other impurities by the iodide method. Therefore, the data

- 2 -

that we obtained in regard to the oxidation kinetics of hafnium refer to a purer metal and is of great interest from the standpoint of investigation of the actual properties of this little-studied and extremely rare metal.

REDUCTION AND PURIFICATION OF METAL. PREPARATION OF SPECIMENS. METHOD OF KINETIC INVESTIGATION

A hafnium powder was obtained from hafnium oxide through reduction by calcium on the basis of the method that was described in [3]. As a result of refining this powder by the iodide method by the procedure developed in our laboratory [4], bars with diameters greater than 2 mm were produced. The bars had a silvery metallic luster, good plasticity and were readily bent (with the characteristic "tin" crack) over a 3-4 mm radius through an angle of 180°. Table 1 shows the results of purification of the hafnium according to the data of chemical and spectral analyses of the initial powder and iodide hafnium. The microhardness of the iodide bars was measured on a PTM apparatus with a load of 100 g; it was 160 units on the average.
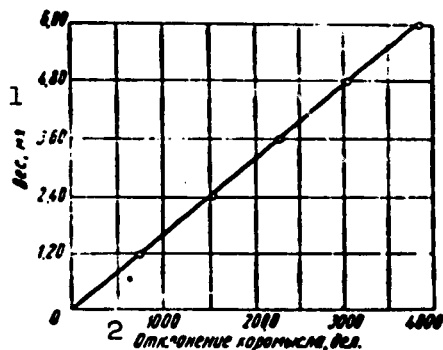
Fig. 1. Calibration diagram for vacuumized torsion microbalance with tungsten thread 50 μ in diameter. 1) Weight, mg; 2) deflection of balance beam, scale divisions.

The iodide hafnium bars were remelted in an argon atmosphere in an MIFI-9-3 electric-arc furnace with a water-cooled copper sole and a tungsten electrode. The hafnium ingot obtained was then rolled in air to a plate thickness of 1.2 mm. After this, the plate was annealed in a vacuum of the order of 10^{-6} mm Hg at a temperature of 800°C for a period of three hours. Analyses of the rolled specimens for gaseous impurities and iron showed the following composition:

- 3 -

0.014% O_2, 0.008% N and 0.01% Fe.

The density of the hafnium obtained, which was found to be 12.98 g/cm^3 (18°C), was determined by the pycnometric method. This corresponds to a zirconium content in the hafnium of less than 1%.

TABLE 1

Results of Analysis of Powder and Iodide Hafnium

1 Элементы	2 Исходный	После йодидной очистки 3
Hf	>99	>99
Zr	<1	<1
Al	0,02	0,008
Ca	0,1	0,02
Si	0,05	0,01
Ti	0,09	0,01
Fe	0,005	0,01
Mn	0,01	<0,005
Cr	0,003	<0,005

1) Element; 2) initial; 3) after iodide purification.

The specimens used for the kinetic investigations were cut from the same sheet and were right-angled parallelepipeds with dimensions of 1 x 7 x 13 mm. Prior to testing, they were carefully polished with emery papers of different grades, down to the finest, and subsequently washed with purified acetone.

The investigation of the oxidation kinetics of hafnium was conducted on a vacuumized torsion microbalance by the continuous suspension method. A description of this balance and the suspension method is given in our paper [5]. Figure 1 shows the results of the calibration of the balance with a torsion element formed by tungsten wire with a diameter of 50 μ.

RESULTS OF INVESTIGATION

The results of the investigation of the oxidation kinetics of hafnium in oxygen under a pressure of 150 mm Hg (which corresponds approximately to the partial pressure of oxygen in air) for the temperature range from 600 to 1000°C is shown graphically in Fig. 2. The ex-

- 4 -

posure time for obtaining the curves of oxidation rate was 10 hours.

The results of analysis of the oxidation-rate curves obtained, from which it follows that the experimental points show good fit to a

Fig. 2. Dependence of weight increase upon time for oxidation of hafnium within temperature range from 600 to 1000°C. 1) Weight increase, mg/cm²; 2) time, hours.

straight line in the corresponding coordinates, are depicted graphically in Fig. 3. We may conclude on the basis of the data in Fig. 3 that at temperatures of 600, 700 and 800°C, the oxidation process conforms to the cubic function

$$y^3 = K_{kub} t + C_1.$$

where y is the weight increase in mg/cm², K_{kub} is the constant of the cubic oxidation function, t is time and C_1 is a constant dependent upon the oxidation temperature.

This function is, however, not correct for the initial oxidation period (15-20 minutes) when the oxidation rate is considerably higher than that of the following period. This phenomenon occurred for all temperatures investigated. It is also generally observed with other metals (Nb, Zr, Ti and others).

- 5 -

At temperatures of 900 and 1000°C, the time dependence of the squares of the weight increases is well represented by a straight line. Therefore, we may consider that the oxidation process at these
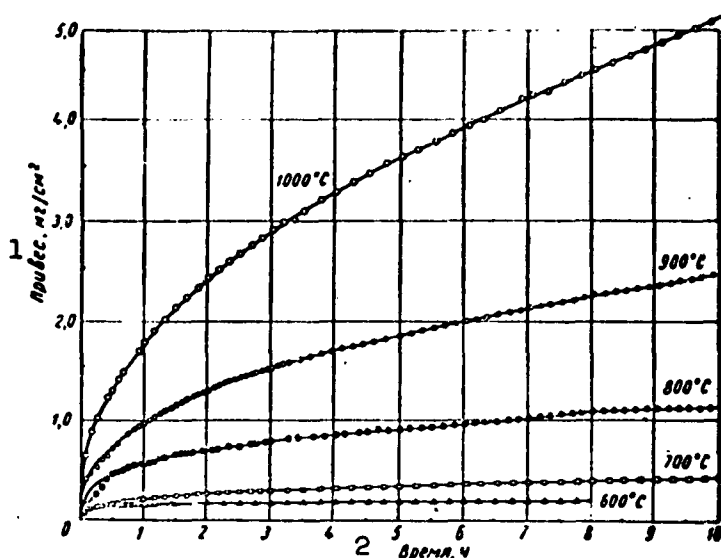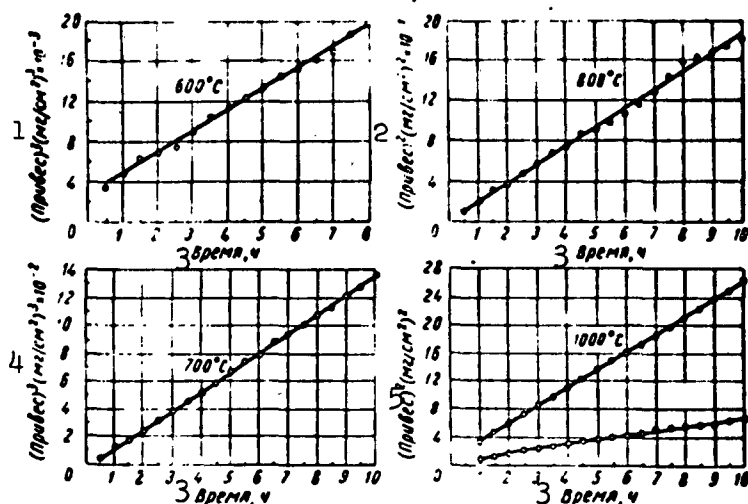

Fig. 3. Dependence of cubes and squares of weight increases upon time in oxidation of hafnium within temperature range from 600 to 1000°C. 1) (Weight increase)^3(mg/cm^2)^3 x 10^{-3}; 2) (weight increase)^2(mg/cm^2)^2 x 10^{-1}; 3) time, hours; 4) (weight increase)^3(mg/cm^2)^3 x 10^{-2}; 5) (weight increase)^2(mg/cm^2)^2.

temperatures corresponds to the parabolic function

$$y^2 = K_{\text{пар}} t + C_2,$$

where K_{par} is the rate constant of the parabolic oxidation function; all the rest of the symbols take the same meanings that they had for the cubic function.

Table 2 shows the oxidation rate constants for different temperatures.

The activation energy of the oxidation process of hafnium, which was found to be 42 kcal/mole, was computed from three values of the oxidation rate constant (K) for the cubic curve, which characterize this process at temperatures from 600 to 800°C. For this purpose, we

constructed a diagram of the relationship of log K to 1/T (where T is the absolute temperature), which is shown in Fig. 4.

TABLE 2

Oxidation Rate Constants of Iodide Hafnium from Cubic $[(g/cm^2)^3/sec]$ and Parabolic $[(g/cm^2)^3/sec]$ Curves

1 Температура, °С	2 Закон окисления в течение 600 мин	3 Константа
600	4 Кубический	$6 \cdot 10^{-10}$
700	»	$4 \cdot 10^{-9}$
800	»	$5 \cdot 10^{-8}$
900	5 Параболический	$7 \cdot 10^{-7}$
1000	»	$2 \cdot 10^{-7}$

1) Temperature, °C; 2) oxidation curve over period of 600 minutes; 3) constant; 4) cubic; 5) parabolic.

A dark-gray monolithic oxide film was observed on the hafnium specimens subsequent to oxidation for a period of 10 hours at all temperatures.
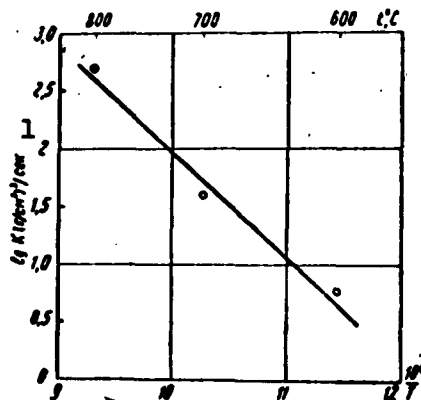
Fig. 4. Relationship of rate constant of cubic law to temperature. 1) log K $(g/cm^2)^3/sec$.

This film was worked by abrasives only with difficulty and was attached firmly to the metal.

The curves of the oxidation rate of hafnium were studied on heating for a period of 110 hours at temperatures of 900 and 1000°C. The results of this investigation are shown in Fig. 5. As is apparent from Fig. 5, two segments may be distinguished on the long-term oxidation curve of the metal. The first segment of the curve depicts the oxidation kinetics for the period when the protective oxide film forms on the surface of the specimen. A reduction in the oxidation rate with the passing of time is observed in

this period. This reduction in the c... rate occurs, as has already been indicated, mainly on a parabolic (or close to it) curve. The second segment of the curve reflects the oxidation kinetics after an oxide film of a certain thickness had formed on the specimen. It
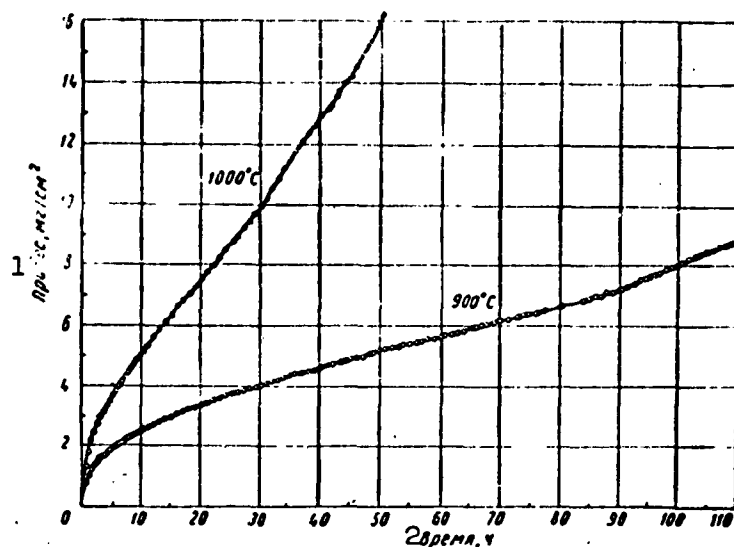
Fig. 5. Dependence of weight increases upon time for 100-hour oxidation of hafnium at temperatures of 900 ana 1000°C. 1) Weight increase, mg/cm^2; 2) time, hours.

characterizes an increase in rate with increasing oxidation time. This increase proceeds up to a certain constant value; then, after a while, the oxidation curve becomes linear. The thickness of the oxide film, after which the oxidation rate begins to increase, is generally termed the "critical" thickness.

For visual observations, the stage of accelerated oxidation begins with formation of a white oxide (Fig. 6a) at the edges of the specimens and on individual zones of the surface. The zones of white oxide expanded with increasing oxidation time to coat the whole surface of the specimen (Fig. 6b). The white oxide layer was brittle and porous.

- 8 -

The maximum weight increases, which correspond to the critical thicknesses of the oxide film for 900 and 1000°C, were 7.26 and 9.99 mg/cm^2, respectively. This difference in weight increase shows that the solid dark-gray oxide film grows (without being converted into the white oxide) to a greater thickness with increasing temperature.
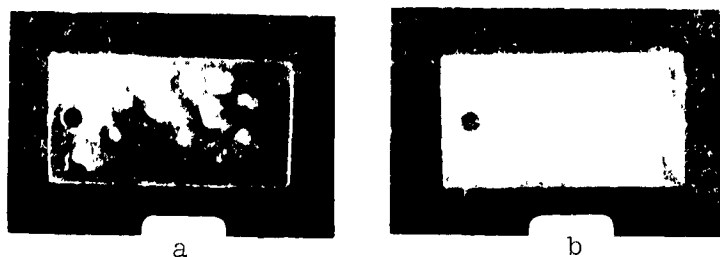
Fig. 6. Hafnium specimens, oxidation at 1000°C. a) For 34 hours; b) for 51 hours.

The curves of the mean oxidation rate for 8 hours as a function of temperature are shown in Fig. 7 and may be used to evaluate the relative stability of hafnium and zirconium. As may be noted, hafnium is considerably more oxidation-resistant than zirconium. A sharp increase in the oxidation rate of hafnium is observed only at a temperature of 700°C, while for zirconium, this temperature is only 500°C.

It is interesting to compare the results of our investigation of the oxidation kinetics of hafnium which had been subjected to iodide purification with analogous data obtained in [2] on hafnium with 5% zirconium.

We may first note the correspondence of the data pertaining to the oxidation kinetics within the temperature range from 900 to 1000°C, where the curves of the oxidation rate conform to parabolic laws. At lower temperatures, however, another evaluation of the oxidation curve of hafnium is obtained. In our work, experimental data on the kinetics were in closer agreement with a cubic curve, while in [2], they agreed with a logarithmic curve. The different evaluations of the oxidation

kinetics of hafnium in the temperature range from 600 to 800°C cannot be referred to the suspension method, since in this temperature range, a balance of approximately the same sensitivity was used in both cases.
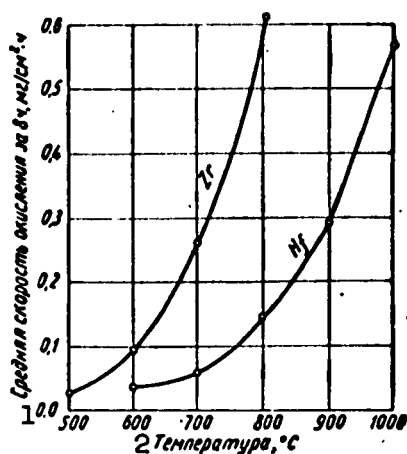
Fig. 7. Dependence of mean oxidation rate of hafnium and zirconium upon temperature. 1) Mean oxidation rate for 8 hours, mg/cm^2· ·hr; 2) temperature, °C.

It remains only to be assumed that the oxidation kinetics of hafnium is dependent essentially upon the contamination of the metal.

At temperatures of 900°C and above, the authors of [2] observed a transition from a parabolic to a linear curve without an increase in the oxidation rate on prolonged holding. In our case, the transition to the linear curve was accomplished through a region of accelerated (as compared with the parabolic curve) oxidation. A bend was detected on the

oxidation-rate curves (see Fig. 5) after a certain time. The analogous phenomenon was observed more distinctly on zirconium [9]. In view of this, the above difference in the oxidation kinetics of hafnium apparently cannot be explained even by the different zirconium contents in the hafnium. We may assume that the authors of [2] failed to observe an increase in the oxidation rate of hafnium subsequent to the parabolic curve as a result of the low sensitivity of the balance used by the authors in this case (5·10^{-4} g/g).

Several attempts have been made to predict a theoretical cubic curve [6, 7], but in specific cases (for example, to explain the oxidation kinetics of tantalum), its use was found to be inappropriate. However, Kubashevskiy and Hopkins [8] consider that the deviation from a clear cubic relationship, which is generally indicated, may be

- 10 -

caused by such secondary effects as, for example, "aging" of the oxide film in the oxidation process. The cubic relationship of the weight increase to time for hafnium that we observed in the present work and that for zirconium [9] show that this relationship occurs for a broader range of metals than was previously assumed.

Recently, temperature ranges in which oxidation of a number of metals (zirconium [9], niobium [10], tantalum [11] and others) proceeds through two distinct stages have been established. The first stage is characterized by the formation and growth of protective oxide films (usually dark gray in color) on the surfaces of the metal. The second stage comes about at a given temperature after the oxide film has attained a certain thickness. This stage is characterized by an increase in the oxidation rate with time due to cracking in the protective film. Here the color of the oxide usually changes from dark gray to yellowish white. According to our data, hafnium may also be referred to this group of metals. There is no consistent opinion concerning the breakdown mechanism of the protective properties of the oxide films on these metals; however, investigators are unanimous in associating the mechanism with the influence of the compressive stresses which form in the oxide film due to the different volumes of the metal and its oxide. As we have shown for zirconium and its alloys [12], the "critical" thickness of the oxide film at which the process of its breakdown begins is dependent essentially upon the yield point of the metallic base. Thus, among other things, the "critical" thickness of the oxide film on zirconium and its alloys increased with increasing temperature. An analogous phenomenon is also observed for hafnium on raising the temperature from 900 to 1000°C.

At temperatures lower than 900°C, we did not observe cracks in the scale on the hafnium; however, we consider that with sufficient

- 11 -

oxidation exposure, this phenomenon may also be observed at lower temperatures when the critical thickness of the oxide film is attained.

CONCLUSIONS

The oxidation kinetics of iodide hafnium in oxygen at temperatures from 600 to 1000°C was investigated by the method of continuous suspension on a highly sensitive vacuumized torsion microbalance. As a result of the investigation, we established that:

1. The oxidation curve of hafnium in the temperature range from 600 to 800°C is expressed by a cubic function of time.

2. At temperatures of 900 and 1000°C, the oxidation curve of hafnium is parabolic for the period of time before the oxide film attains a critical thickness. Subsequent to this, cracking of the oxide film is also observed and, as a result, an increase in the oxidation rate.

3. The increase in the oxidation rate (break on kinetic curve) is coincident with the transformation of the dark oxide film into a white oxide.

REFERENCES

1. Lastmen, B. and Kerze, F., Metallurgiya tsirkoniya [Metallurgy of Zirconium], Moscow, Izd-vo inostr. lit. [Foreign Literature Publishing House], 1959.

2. Smeltzer, W., Simnad, M., Acta metallurgica, 5, No. 6 (1957).

3. Ruff, O. and Brintzinger, H., Z. anorgan. und allgem. Chem. [Journal of Inorganic and General Chemistry], No. 129, 267 (1923).

4. Yemel'yanov, V.S., Bystrov, P.D. and Yevstyukhin, A.I., Sb. Metallurgiya i metallovedeniye chistykh metallov [Metallurgy and Physical Metallurgy of Pure Metals], No. 1, Izd. MIFI [Publishing House of the Moscow Physics and Engineering Institute], 1959.

5. Revyakin, B.N., Korobkov, I.I., Yevstyukhin, A.I. and Lyashenko,

V.S., Sm. nastoyashchiy sbornik [see present collection].

6. Uhlig, H.H., Acta Metalurgica, No. 4 (1956).

7. Engell, H., Hauffe, K. and Ilschner, B., Elektrochem. [Electro-chemistry], 58 (1954).

8. Kubashevskiy, O. and Gopkins, B., Okisleniye metallov i splavov [Oxidation of Metals and Alloys], Moscow, Izd-vo inostr. lit [Foreign Literature Publishing House], 1955.

9. Korobov, I.I., Dissertation (Elektronograficheskoye i kineti-cheskoye issledovaniya tsirkoniya i yego splavov). [Dissertation. (Electronographic and Kinetic Investigations of Zirconium and Its Alloys)], Izd. MIFI, 1959.

10. Gulbransen, A. and Andrew, K., J. Metals, No. 3 (1953).

11. Cathcart, J., Bakish, R., Norton, D, J. Electrochem. Soc., 107, No. 8 (1960).

12. Korobkov, I.I. and Yevstyukhin, A.I., Sb. Metallurgiya i metallov-edeniye chistykh metallov, No. II, Moscow, Atomizdat [Nuclear Research Publishing House], 1960.

Manu-script Page No.	[List of Transliterated Symbols]		
5	куб = kub = kubicheskiy = cubic
6	пар = par = parabolicheskiy = parabolic

ZONE MELTING OF NIOBIUM BY THE ARC METHOD

A. I. Yevstyukhin, V. V. Nikishanov and I. V. Milov

INTRODUCTION

As a high-melting metal with good technological and nuclear properties, niobium has become increasingly attractive for a number of ramifications of modern technology. During the past five years, a large number of investigations in different parts of the world have been devoted to the study of niobium and its alloys.

The principal disadvantage of niobium as a structural material is its low high-temperature corrosion resistance in air, which drops particularly sharply in technical grades of the metal, which contain large quantities of impurities. Impurities in niobium, particularly nonmetallic (carbon, oxygen, hydrogen etc.) impurities, also sharply reduce the technological properties of the metal; this is extremely important for its technological use. Therefore, methods of purifying niobium of its accompanying impurities continue at all times in the foreground of developing niobium metallurgy. The methods of purification determine, to a certain extent, the production and application of niobium.

At present, the most promising methods of purifying niobium of impurities are considered to be refining melting in a high vacuum and zone melting by the arc or electron beam methods. Certain investigators [1] have employed so-called "cellular" zone melting of niobium with the use of high-frequency melting for this purpose.

Zone melting with a low-voltage arc discharge guarantees the pos-

sibility of obtaining a comparatively narrow molten zone with a concentrated feed of required power through the arc and rapid transfer of heat from the boundaries of the zone. Vigorous dissipation of heat from the zone is accomplished in a copper water-cooled crucible, taking advantage of the high thermal conductivity of copper, with which the molten metal does not react. The method of arc zone melting in a copper crucible is attractive for its simplicity, low cost and the possibility of using it on a large industrial scale. However, like the method of induction zone melting, it has a disadvantage consisting in the difficulty of stable power supply, which plays a major role at low zone speeds.

The present study undertakes the task of experimental investigation and verification of the feasibility of arc zone melting of niobium, which was conducted on an apparatus that was specially designed in our laboratory. The distribution of impurities in zone melting was studied through the behavior of carbon, silicon, iron and lead as impurities that react differently with niobium. Generally, purification from impurities could be predicted in zone melting of niobium from knowledge of the "niobium corner" of the diagram of state of niobium with impurity elements [2, 3]. The available diagrams of state [4, 5] enable us to solve in principle the problem of the applicability of zone refining for certain impurities such as carbon, silicon, titanium, tungsten, molybdenum, tantalum, vanadium and several others. For example, carbon forms a solid solution with niobium below 0.02 atom-% and may be separated out by zone refining. Titanium forms a continuous series of solid solutions with niobium. Highly effective purification of niobium from titanium is possible in view of the low dispersion coefficient. According to the diagram of state of the niobium — silicon system, the separation of niobium and silicon may also be attained by

the method of zone melting. Data on the diagram of state of niobium –
lead have not been published. Again, nothing is known of the nature of
the interaction of niobium with small lead additives. Proceeding from
the physical-metallurgical premises for the formation of solid solu-
tions, however, it is difficult to anticipate that lead will undergo
pronounced solution in niobium.

Thus the knowledge available at present on the diagrams of
state of niobium with the above elements and the absence of the nec-
essary data prevent our determining the extent of purification with
zone melting by calculation. Experimental investigations are required
for this purpose.

APPARATUS FOR ARC ZONE MELTING

The apparatus used for arc zone melting (Fig. 1) consists of a
melting chamber, the vacuum system for the chamber, a system for puri-
fying the argon and filling the chamber, a power source for the arc
and a mechanism to advance the molten zone. We used an MIFI-9-3 arc
furnace with an attachment for zone melting. This attachment consisted
of an electrode-displacement system and a ring-shaped copper crucible.
The crucible had a circular groove with a partition for specimens with
lengths to 230 mm and a dished depression in the center for a getter.
The crucible and electrode were cooled vigorously with water. The
mechanical system for electrode displacement at a preset rate was
mounted on the housing of the arc furnace. It consisted of an electric
motor, a reducer with discontinuous speed control, and a mechanism for
displacement and adjustment of the gap between the electrode and ingot.
Three columns support a bearing ring in which a gear pair turns. The
larger gear of this pair has a groove in which the articulated adjust-
ing head was displaced. The electrode passed through the head. Varia-
tion of the radius of the circle through which the electrode is dis-

Fig. 1. General appearance of apparatus used for arc zone melting.

placed was accomplished by moving the articulated head along the groove. Rotation of a nut raised or lowered the electrode. Airtightness was secured in the system with bellows and a rubber vacuum seal.

The smelting chamber of the furnace was connected to a forevacuum pump and the purification system for the inert gas. The attachment used enables us to conduct smelting in either an inert atmosphere or a vacuum. We conducted the zone melting of niobium in an atmosphere of argon since the arc will burn more steadily in argon than it will in a vacuum and a narrow molten zone is produced. To purify the argon of moisture and

Fig. 2. Niobium specimen after zone leveling.

impurities, we passed it through $CaCl_2$ and heated shavings of metallic calcium and metallic zirconium.

TESTS ON ARC ZONE MELTING OF NIOBIUM

Technical-purity niobium served as the initial material for zone melting. The impurity content in the niobium did not exceed the values given in Table 1.

The material in the form of individual melted fragments and filings with a total weight to 150 g was poured into the circular groove

TABLE 1

Impurity Content in Niobium

[1] Элемент	[2] Вес. %	[1] Элемент	[2] Вес. %
Кислород [3][4]	0,008	Углерод [8]	0,060
Водород [5]	0,007	Железо [9]	0,08
Азот [5][6]	0,012	Титан [10]	0,150
Свинец [7][6]	0,030	Кремний [11]	0,080
Хром [7]	0,040		

1) Element; 2) % by weight; 3) oxygen; 4) hydrogen; 5) nitrogen; 6) lead; 7) chromium; 8) carbon; 9) iron; 10) titanium; 11) silicon.

and fused together into a monolithic specimen. This specimen was subjected to zone melting for ten passes in the forward and reverse directions with a speed of 0.5 mm/sec in order to render composition uniform over the length of the specimen. After zone leveling, a control specimen 5-10 g in weight, from which we determined the initial hardness and chemical composition of the specimen after completion of the process, was cut from the ingot with the arc without opening the furnace.

The furnace was connected with the argon-purification system at all times during the melting. Prior to starting the melting and before each pass, an iodide-zirconium getter was melted for an extended period. These measures should have contributed to most complete elimination of the oxygen and nitrogen from the argon and the surfaces of the furnace and crucible.

Five specimens, each with a length of 230 mm and a diameter of 15 mm, were subjected to zone melting; the width of the zone was 20 mm. The zone speed was the same for all specimens at 0.5 mm/sec. The number of zone passes was varied for each specimen with 16, 32 (two specimens), 64 and 128 passes, respectively. After each pass, the specimens were inverted and zone melting was carried out on the undersides.

The purpose of the tests was a qualitative detection of the puri-

fication effect; therefore, such simple methods as studying the variation in hardness over the length of the specimen and metallographic and chemical analyses were employed as controls. In one case, the radioactive-isotope method was employed to study the distribution of carbon in the niobium in zone purification. For this purpose, we used the radioactive carbon isotope C^{14}.

Fig. 3. External appearance of niobium specimen after zone refining. Zones from which sections were made are keyed by dots.

The specimens, which were subjected to directional zone melting, differed in external appearance from the specimens of leveled composition (see Fig. 2). The front zone of the ingot had a smooth lustrous surface, while that of the rear zone was dull, rough and occasionally had a large shrinkage cavity or conical mound. The reason for this is apparently the transfer of the gaseous and other impurities. The front zone of the ingot was larger than the rear due to transfer of metal. This may be prevented by appropriate tilting of the crucible.

Very long crystals grew out from the walls and bottom of the crucible toward the axis of the specimen in the direction of zone movement. The grains in the front zone of the ingot were larger and more elongated than those in the rear zone. Microsections of the specimens were identical for ingots with different numbers of zone passes.

Metallographic analysis of the ingots shows that as we approach the front and rear zones, an extension of the grain boundaries, a decrease in grain size and the appearance of foreign inclusions (probably of a second phase) are noted. The largest and purest grains are

near the front end of the ingot at a distance 1/3 the length of the specimen. Figure 4 shows the microsections of the zones which are keyed by the points in Fig. 3. The specimen was subjected to 32 passes. The diagrams of the variation in hardness over the length of the spe-
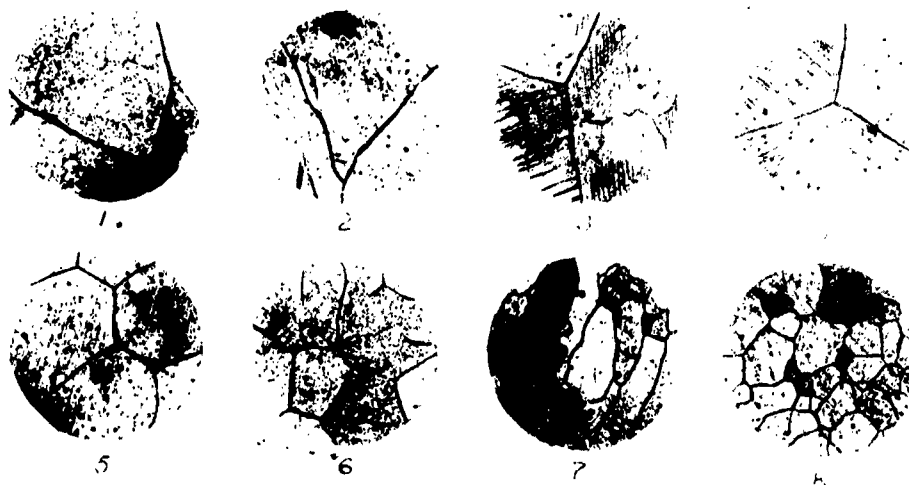
Fig. 4. Microsection of zones of ingot subjected to 32 passes (zones are keyed by dots in Fig. 3).

cimens (Fig. 5) supplement the metallographic data. The distances from the front end of the ingot in the direction of zone movement are plotted against the axis of abscissas, while the hardness values are plotted against the axis of ordinates. The dash line designates the hardness level of the specimen prior to zone melting. A comparison of the curves for specimens with different numbers of passes shows that the relative zone of an ingot having reduced hardness as compared with the initial hardness increases in size with increasing number of passes.

Chemical analysis of niobium specimens that were subjected to zone refining at a zone speed of 0.5 mm/sec shows that substantial purification of the niobium of silicon, titanium and iron did not occur. Obviously, this is explained by the high zone speed, at which purifi-

cation from the above impurities, which have distribution coefficients that differ little from unity, does not occur (the distribution coefficients for silicon and titanium were determined from the diagram of state; here they were found to be 0.25 and 0.5, respectively).
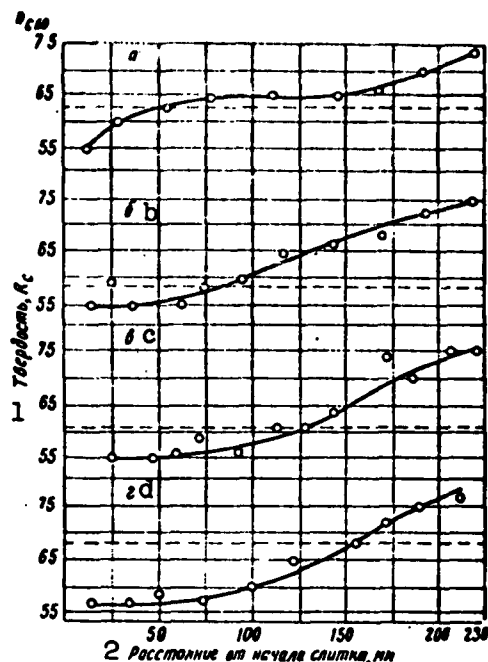

Fig. 5. Curves of hardness distribution of niobium after 16 (a), 32 (b), 64 (c) and 128 (d) zone passes with zone width of 20 mm, ingot length of 230 mm and zone speed of 0.5 mm/sec. 1) R_c hardness; 2) distance from front of ingot, mm.

Interest is drawn to data from chemical analysis for the distribution of lead over the length of the specimens after zone refining with different numbers of passes. The distribution curves of the lead are shown in Fig. 6. The chemical analysis shows marked purification of the niobium from the lead. After purification, the lead impurities were concentrated in the rear zone. The purification effect increases with increasing number of passes, although there is no noticeable variation in the length of the purified zone of the ingot. We failed to determine the distribution coefficient of the

lead impurity in the niobium, because the Nb–Pb state was not studied.

Pfann [6] gave a formula describing the distribution of impurities after a single pass:

$$C = C_0 [1 - (1 - k) e^{-kx/l}] \qquad (1)$$

where C is the impurity concentration at point $\underline{x}$, C_0 is the initial concentration of impurities in the specimen, $\underline{l}$ is the length of the

- 21 -

zone and $\underline{k}$ is the distribution coefficient of the impurities.

The equation that Pfann gives for the impurity content in a specimen after zone refining with $\underline{n}$ passes is cumbersome and inconvenient in calculations.

V. I. Vigdorovich and V.S. Ivleva [7] proposed a relatively simple graphical method for determing the distribution coefficient after $\underline{n}$ zone passes. The equation for $\underline{n}$ zone passes appears as follows:

$$C_n = C_0 \left[1 - (1 - k) e^{-kx/l} \right]^n,$$

hence,

$$\frac{1}{1-k}\left(1 - \sqrt[n]{\frac{C_n}{C_0}}\right) = e^{-kx/l}; \tag{2}$$

denoting the left member by $\underline{x}$ and the right member by $\underline{y}$, we construct for them the curves

$$x = f(k), \quad y = \psi(k).$$

The intersection point of these curves corresponds to the effective value of the distribution coefficient $\underline{k}$.

Formulas (1) and (2) are correct for equilibrium states of the process. But with certain allowances the formulas may also describe the nonequilibrium processes of zone melting with sufficient accuracy. The values of the distribution coefficient of lead in niobium were 0.80, computed from the test data for a specimen after 64 zone passes, and 0.71 for a specimen after 32 zone passes.

Data of chemical analysis and the computed value of the distribution coefficient provide certain grounds for the assumption that lead forms solid solutions with niobium with melting points lower than that of pure niobium, and that these are displaced to the end of the ingot under the influence of zone melting.

Moreover, it is possible that sufficient diffusion of the lead in the molten zone of the niobium cannot take place under certain melting
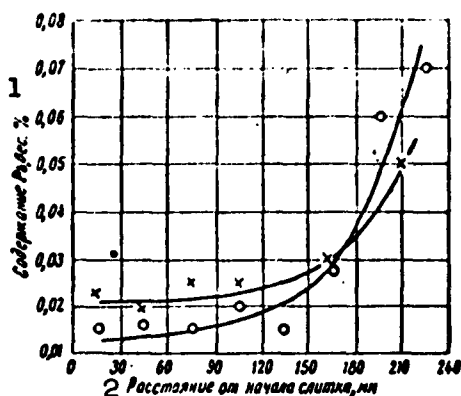
Fig. 6. Curves of lead distribution in niobium (direction of zone movement is from left to right relative to distribution curve). x) After 32 zone passes; 0) after 64 zone passes. 1) Pb content, % by weight; 2) distance from front of ingot, mm.

conditions. This suggests that lead may have a low diffusion coefficient in niobium in the liquid phase. However, an independent investigation is necessary for final solution of this problem.

Chemical analysis for carbon did not show any noticeable change in its distribution in the niobium specimens after melting at a zone speed of the order of 0.5 mm/sec. Thus, for a specimen subjected to 32 passes with a speed of 0.5 mm/sec, the carbon content at points which are equally spaced at a distance of approximately 25 mm from one another is given in Table 2.

TABLE 2

Carbon Content in Different Zones of Specimen Subjected to 32 Passes

1 Номер участка	1	2	3	4	5	6	7
2 Содержание углерода, %	0,058	0,058	0,08	0,08	0,06	0,066	0,07

1) Zone No.; 2) carbon content, %.

More accurate data on the distribution of carbon was obtained with the radioactive isotope C^{14}, which emits soft β^--radiation, than was obtained by the chemical analysis. 0.01 percent of the C^{14} isotope was introduced into a specimen with an initial carbon content of 0.05% by weight. The specimen was first subjected to zone leveling. Then directional zone melting was conducted. Thirty-two passes were made. Measurements of the radiation intensity were made with an end-window

counter through an aperture in a lead diaphragm under which different zones of the ingot were placed. The results of measurement of the radiation intensity are presented in the form of a graph in Fig. 7.
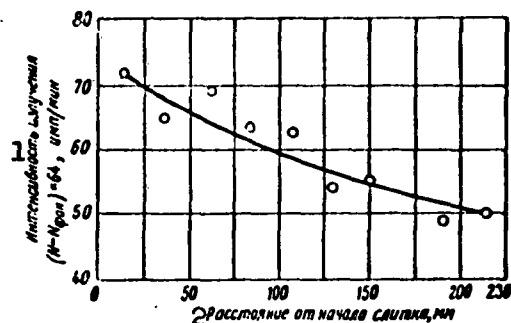

Fig. 7. C^{14} distribution in niobium specimen after zone refining (number of passes 32, zone speed 0.5 mm/sec and length of zone 20 mm). 1) Radiation intensity $(N-N_{background})\cdot \cdot 64$, pulses/min; 2) distance from front of ingot, mm.

The experiment showed that the distribution coefficient of carbon in niobium is greater than unity, i.e., the carbon is concentrated in the front zone of the ingot and moves against the motion of the zone. Chemical analysis (Table 3) shows that purification of niobium of Si, Ti and Fe was not observed under the given zone-melting conditions. Obviously, the effective distribution coefficients of these impurities in niobium are close to unity and a vast number of passes (cycles) is required for the niobium to undergo pronounced pu-

TABLE 3

Data from Chemical Analysis of Specific Zones of Niobium Specimens After Zone Melting

[1]Количество проходов	[2]Номер участка	Ti	Si	Fe	[1]Количество проходов	[2]Номер участка	Ti	Si	Fe
32	1	0,12	0,055	0,09	64	1	0,12	0,08	0,08
	2	0,075	0,05	0,09		2	0,16	0,05	0,08
	3	0,075	Следы[3]	0,09		3	0,15	0,06	0,08
	4	0,012	0,05	0,09		4	0,12	0,07	0,085
	5	0,075	Следы	0,08		5	0,12	0,045	0,08
	6	0,075	0,06	0,08		6	0,13	Следы	0,08
	7	0,09	0,05	0,09		7	0,13	Следы	0,08
	8	0,12	0,05	0,09					

1) Number of passes; 2) zone No.; 3) traces.

rification from the impurities under these conditions.

CONCLUSIONS

1. An apparatus for zone melting of high-melting metals by the electric-arc method was built and tested. The tests and subsequent work showed the apparatus to perform reliably during its operation.

2. Tests were conducted in the purification of niobium by the zone method. An effect of purification from lead and carbon was detected at a zone speed of 0.5 mm/sec. Under more favorable conditions (reduced zone speed and molten-zone width), zone refining with the use of an arc may obviously be found more effective.

3. The test results show that under certain melting conditions (v = 0.5 mm/sec and $\underline{1}$ = 20 mm), the purification limit is not attained even after 120-130 passes.

4. The radioactive isotope method is highly effective for detecting the purification effect. In combination with other methods, the radioactive isotope method substantially facilitates and accelerates monitoring of the processes in zone melting.

5. The authors propose that to conduct purification of niobium successfully by the method of arc zone melting, it is necessary to use a speed 5-10 times lower than that used in the above work; these speeds should be a few millimeters per minute, i.e., they should approximate the speeds employed in induction zone melting of low-melting metals. For this purpose, the authors designed an apparatus for arc zone melting with molten-zone advance speeds of a few millimeters per minute.

REFERENCES

1. Industr. Heat, No. 5, 924 (1958).
2. Vigdorovich, V.N., Krapukhin, V.V. and Chernomordin, I.F., Izv. AN SSSR, Otd. Tekhn. nauk. Metallurgiya i toplivo [Publishing House of the Acad. Sci. USSR, Division of Technical Sciences,

Metallurgy and Fuel], No. 4, 99 (1960).

3. Vigdorovich, V.N., Ivleva, V.S. and Krol', L.Ya., Izv. AN SSSR, Otd. tekhn. nauk. Metallurgiya i toplivo, No. 1, 44 (1960).

4. Hansen, M., Anderko, K., Constitution of binary alloys, 1958.

5. Samsonov, G.V. and Konstantinov, V.N., Tantal i nioby [Tantalum and Niobium], Moscow, Metallurgizdat [State Scientific and Technical Publishing House for Literature on Ferrous and Nonferrous Metallurgy], 1959.

6. Pfann, W., Zone Melting, N.Y. (1958). Russian translation: Pfann, V.Dzh., Zonnaya plavka [Zone Melting], Moscow, Metallurgizdat, 1960.

7. Vigdorovich, V.N. and Ivleva, V.S., Izv. AN SSSR, Otd. tekhn. nauk., Metallurgiya i toplivo, No. 1 (1961).

INVESTIGATION OF THE OXIDATION KINETICS OF NIOBIUM

IN THE TEMPERATURE REGION FROM 500 to 1000°C

B. N. Revyakin, I. I. Korobkov, A. I. Yevstyukhin

and [Deceased] V. S. Lyashenko

Niobium possesses a whole series of valuable properties: high heat resistance, a relatively small capture section for thermal neutrons, good compatibility with uranium, a high corrosion resistance in liquid-metal heat carriers and good technological properties; these are indicative of the promising nature of its use. In recent years, many studies [1-5] devoted to study of the oxidation process of niobium have been published; however, the mechanism of the process remains unclear in many respects.

Gulbransen and Andrew [1] studied the interaction of niobium with oxygen by the method of continuous suspension on a vacuumized torsion microbalance. They found that the oxidation follows a parabolic curve in the temperature range from 200 to 375°C under an oxygen pressure of 7.6 cm Hg. The activation energy of the process was found to be 22,800 cal/mole.

Bridges and Fassel [2] investigated the oxidation of niobium at temperatures of 400-800°C and under oxygen pressures from 1 to 40 atm.

According to their data, beginning at a certain moment, the oxidation of niobium follows a linear curve at the temperatures under consideration; here the period of time after which the transition to a linear curve is observed decreases with increasing temperature from six hours at 400°C to a few minutes at 500°C (under an oxygen pressure

of 1 atm). The oxidation rate of niobium increases sharply with increasing oxygen pressure at 550-650°C. According to the data of the authors, the oxidation rate decreases under oxygen pressures from 1 to 40 atm with increasing temperature from 575 to 650°C, i.e., the oxidation rate has a maximum at 575° and a minimum at 650°C. The activation energy according to their determination is 9-10 kcal/mole (at 500-800°C).

In a more recent work by Gulbransen and Andrew [3], the oxidation of niobium was investigated in the temperature region from 375 to 700°C under an oxygen pressure of 7.6 cm Hg.

It was established that a transition from the parabolic oxidation curve to the linear law at a temperature of 400-450°C is observed at a film thickness corresponding to a weight increase of 50-70 mg/cm^2, i.e., approximately 80 minutes after the start of oxidation.

The authors explain the disappearance of the film's protective properties, i.e., the transition to the linear oxidation curve, by loss of adherence of the oxide film to the metal, which was observed on individual zones. The fact that the oxidation rate decreases with increasing temperature from 550 to 650°C, which was detected by Bridges and Fassel, is not confirmed in this work.

In [4], the oxidation of niobium was investigated in oxygen (under a pressure of 1 atm) and in air at temperatures of 600-1200°C. It was established that niobium oxidizes linearly in oxygen at all temperatures investigated; the activation energy in the range from 600 to 1100°C is 5410 cal/mole; extrapolating the data obtained at lower temperatures, the oxidation rate above 1100°C becomes greater than what we would have expected.

Thus, as is apparent from this short synopsis, data on the oxidation kinetics of niobium are incomplete and highly contradictory.

The purpose of the present work was systematic investigation of the oxidation kinetics of niobium in pure oxygen in a broad temperature range under a pressure of 150 mm Hg; this corresponds approximately to the partial pressure of oxygen in air.

METHOD OF INVESTIGATION

The investigation of the oxidation kinetics of niobium was conducted by continuously recording the weight increase in specimens at constant temperature as a function of the heating time on a special vacuumized torsion microbalance. The working principle of the balance is depicted schematically in Fig. 1. The torsion filament was prepared from tungsten wire 100 and 150 μ in diameter. A quartz balance beam 110 mm long was fused with silver chloride to the middle of the thread; the specimen and counterweight were suspended from the ends of the balance beam on quartz filaments. The specimen to be examined was attached to a quartz hook with platinum wire 0.1 mm in diameter. Calibration and operational checking of the balance showed that its sensitivity was $7 \cdot 10^{-6}$ and $4 \cdot 10^{-5}$; the reproducibility of the suspension results was wholly satisfactory (Fig. 2). Readings of the balance-beam displacement were made with a special CMS-6 optical measuring device that enables us to measure displacements with an accuracy to 0.001 mm. A steady vacuum of the order of 10^{-6} mm Hg was created in the balance prior to admission of oxygen. Oxygen was released into the balance after the required specimen temperature had been reached. A quartz tube in which the specimen to be examined was held was placed in a special tubular furnace with a bifilar winding, the temperature of which was maintained with EPV-01 thermoregulators with an accuracy of $\pm 3^{\circ}C$. The oxidation temperature was measured with the use of a platinum/platinum-rhodium thermocouple in the immediate vicinity of the specimen.
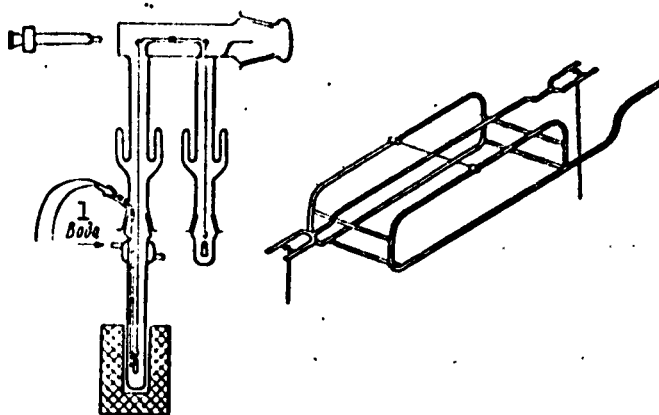
- 29 -

Fig. 1. Principle of vacuumized microbalance. 1) Water.

The oxygen was produced by decomposing previously degasified crystals of potassium permanganate by heating them in vacuo; the oxygen was passed through a U-tube with a filter made from glass wool and
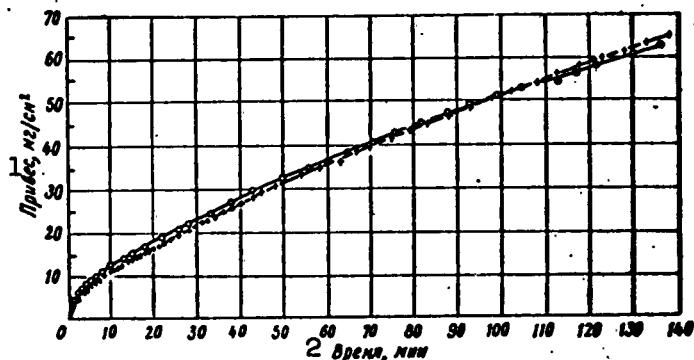
Fig. 2. Reproducibility of results on oxidation of two niobium specimens (T = 800°C; P_{O_2} = 150 mm Hg). 1) Weight increase, mg/cm^2; 2) time, min.

a trap with liquid nitrogen for the purposes of purification and drying.

The niobium specimens to be examined were rectangular parallelepipeds with dimensions of 20 x 10 x 1 mm. Prior to examination, the specimens were polished on successive emery papers with gradually de-

- 30 -

creasing grain size down to No. 20 and subsequently rinsed with ace-
tone. Technical rod niobium, which was remelted in a vacuumized arc
furnace and subsequently cold-rolled into a sheet 1 mm in thickness
served as the material for the investigation. Chemical analysis of the
remelted niobium produced the following results 99.9% Nb, 0.027% O,
0.0004% H, 0.002% N and 0.01% C.

The cast metal had a hardness of 110-120 H_B; the hardness of the
metal after rolling was 240 Brinell units.

RESULTS OF THE INVESTIGATION

The results of kinetic investigation of the oxidation of niobium
in the temperature range from 500-1000°C are shown in Fig. 3.
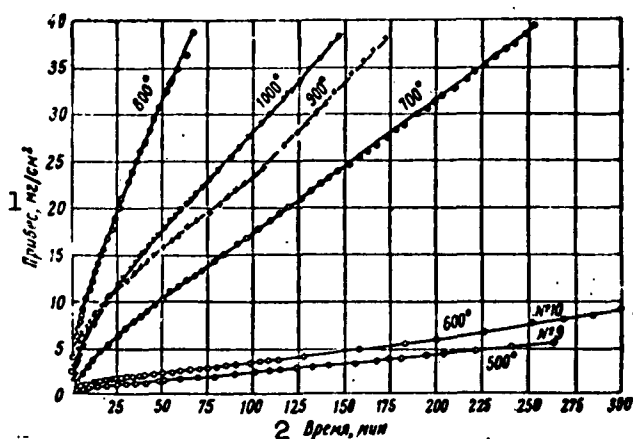
Fig. 3. Oxidation curves of niobium in
oxygen under pressure of 150 mm Hg in
temperature region from 500 to 1000°C.
1) Weight increase, mg/cm^2; 2) time,
min.

It is necessary to note that the kinetic investigation data shown
in Fig. 3 were obtained on niobium specimens of the same melt. Inves-
tigation of the oxidation of niobium of various melts showed that the
oxidation rate of niobium varied sharply (to 150%) from one melt to
another. This shows that even when present in niobium in small quanti-
ties (~0.1%), impurities may affect the oxidation kinetics of niobium

- 31 -

very strongly.

The oxidation of niobium in oxygen (P_{O_2} = 150 mm Hg) occurs linearly in the temperature range investigated with the exception of the initial period, in the course of which the oxidation rate takes higher values than in the following period.

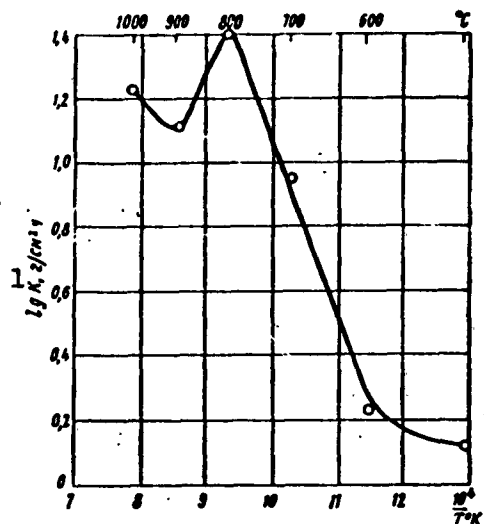Fig. 4. Dependence of constant of linear oxidation curve on temperature. 1) log K, g/cm^2·hr.

Figure 4 shows the dependence of the logarithm of the constant of the linear oxidation curve of niobium (K) upon the reciprocal of the absolute temperature.

It is apparent from Fig. 4 that only three logarithmic values of the constant of the linear oxidation curve, which were obtained from the kinetic oxidation curves of niobium at temperatures of 600, 700 and 800°C, fit satisfactorily on the straight line.

We may conclude from this that in contrast to the majority of metals, Arrhenius' equation (K = Ae$^{-Q/RT}$, where A and R are constants, Q is the activation energy and T is the absolute temperature) is valid for the oxidation of niobium only for a narrow temperature range (600-800°C). The activation energy of the oxidation process of niobium, which was found to be 25 kcal/mole, was computed from the diagram in Fig. 4 for this temperature range. On temperature variation in the range from 500-600°C, the oxidation rate of niobium increases more slowly than we would have expected on extrapolating the Arrhenius line for lower temperatures.

On increasing the temperature above 800°C, a sharp break in the

line with a distinct minimum at 900°C is observed on the diagram. The oxidation rate at this temperature was found to be approximately half that at 800°C.

After a certain oxidation time — characteristic for each temperature — a light-yellow, porous, brittle oxide appeared on the surfaces of the specimens. Beginning with this moment, the scale on the specimens became double-layered. The layer thickness of the light-yellow oxide increased with time, while the thickness of the dark film remained approximately the same.

Fig. 5. External appearance of niobium specimens oxidized for 1 hour at temperature of 800 (a) and 900 (b)°C. In center, niobium specimen; at sides, scale.

It is necessary to note that the nature of the scale changes with changing temperature. The light oxide film which forms on the surfaces of the specimens at 700°C and below crumbles to irregular plates during rapid and slow (with the furnace) cooling. The formation of a brown oxide film, which is securely attached to the base metal and does not peel off on cooling, was observed on the faces of the specimens at 800°C; on the faces, the oxide film has deep cracks running longitudinal to the edges; here, unlike the scale on the edges, it has a light-yellow color and peels off when cooled (Fig. 5a). A characteristic

property of the oxidation process at $900^\circ C$ and above is sintering of the oxides, so that the scale that peels off on cooling exactly retains the shape of the specimen (Fig. 5b).

To ascertain the direction of diffusion of the re-agents in formation of the scale, the following test was conducted. A thin layer of gold was applied to the surface of niobium specimens by vaporization and condensation in vacuo. Subsequent to this, the specimen was subjected to oxidation at $600^\circ C$ for a period of 3 hours. In the oxidation process, the thin gold layer, which is an inert marker in this experiment, remained on the surface of the specimen. This shows that the oxidation of niobium occurs as a result of the diffusion of oxygen ions through the oxide layer.

DISCUSSION OF RESULTS

Data relating to the oxidation kinetics of arc-melted and cold-rolled niobium were obtained in this study for the temperature range from $500-1000^\circ C$. The selection of this temperature range was dictated mainly by the contradictions in the results obtained from various investigations in the temperature region from $550-650^\circ C$ and inadequate study of the oxidation kinetics of niobium at $800-1000^\circ C$.

As a result of the present investigation, it was established that the isothermal oxidation process of niobium is described by a linear law in the range from $500-1000^\circ C$; this fact agrees with data of other investigators. However, we did not observe a reduction in the oxidation rate due to a rise in temperature in the range from $550-650^\circ C$, as is noted in [2]. According to our data (Fig. 4), the constant of the oxidation reaction of technical niobium increases in this temperature range; this agrees with the results obtained by Gulbransen and Andrew [3].

In a higher temperature region, however, we did observe an anom-

aly in the temperature relationship of the oxidation constant analogous to that noted in [2]. According to our observations, the oxidation rate of niobium is reduced by approximately one-half on increasing the temperature from 800 to 900°C. Such a significant difference in the temperature range of the anomalous oxidation-rate variation is highly essential and is linked with the difference in the degree of purity and initial states of the niobium employed in our work and those cited above.

Fig. 6. X-ray pattern of scale from niobium specimens that were oxidized for 1 hour at temperatures of 800 (a) and 900 (b)°C. ($Cu_{K\alpha}$, 40 kv, RKU – $\emptyset$ 114 mm).

We should note that there are no adequately reliable data in the literature for the temperature region from 800-1000°C. The precision investigations of Gulbransen and Andrew [1, 3] include only the temperature region from 200 to 700°C. Bridges and Fassel [2] published data relating to the oxidation of niobium in the temperature region from 400 to 800°C. The investigations made in [4], although conducted in a wide temperature region (600-1200°C), had a larger interval – 200°C.

We established that in the temperature range from 800 to 900°C, the oxidation rate of niobium does not increase with increasing temperature as at other temperatures, but decreases. The transition from $\alpha\text{-Nb}_2\text{O}_5$ to $\beta\text{-Nb}_2\text{O}_5$ occurs at these same temperatures. According to the x-ray data of Goldschmidt [5], the oxide $\alpha\text{-Nb}_2\text{O}_5$ (the metastable modi-

- 35 -

fication) forming on oxidation of niobium undergoes an irreversible polymorphic transformation on isothermal holding. The time of this transformation is dependent upon the temperature, and below $800^\circ C$, the transformation proceeds so slowly that it does not occur in the exposure periods generally employed to investigate the oxidation of niobium. At a temperature above $800^\circ C$, this process takes place at a faster rate, as a result of which in this case, the stable modification $\beta\text{-}Nb_2O_5$ forms on the niobium surface in the oxidation process.

According to our data (Fig. 6), which were also obtained by the x-ray method, a scale corresponding to $\alpha\text{-}Nb_2O_5$ forms on niobium specimens that undergo oxidation at temperatures of $500\text{-}800^\circ C$, while the scale consists of $\beta\text{-}Nb_2O_5$ at temperatures of $900^\circ C$ and above.

This circumstance leads us to assume the presence of a link between the oxidation kinetics and the structure of the oxide on the surface of niobium.

The reduction in the oxidation rate with increasing temperature from 800 to $900^\circ C$ may also be explained by other processes which occur in the oxide film and mainly by the sintering of the oxides, which was clearly observed at temperatures above $800^\circ C$.

In conclusion, we should note that for comprehensive evaluation of the causes of the niobium oxidation anomaly which was noted in the study, it is expedient to study the physicochemical properties of the oxide which forms on the surface of niobium at various temperatures.

REFERENCES

1.   Gulbransen E. and Andrew K. J. Inst. Metals, 188, 586-599 (1950).

2.   Baur J., Bridges D. and Fassel W. J. Eletrochem. Sci., 103, No. 6 (1956).

3.   Gurbransen E. and Andrew K. J. Inst. Metals, March 1953.

4. Klopp W., Simms C., Jaffee R. Trans. Amer. Soc. Metals, 51, 282 (1959).

5. Goldschmidt H. J. Inst. Metals, 87, No. 7 (March 1959).

MODULUS OF ELASTICITY OF BERYLLIUM

AT ELEVATED TEMPERATURES

A. N. Semenikhin, P. L. Gruzin and D. M. Skorov

INTRODUCTION

In recent years, growing interest has been turned to beryllium as a promising material for nuclear power engineering and other fields. This interest was due largely to its unique physical properties, such as low specific gravity, high modulus of elasticity and a high strength-to-specific gravity ratio. Beryllium is an excellent neutron moderator and reflector. It has an extremely small capture section for thermal neutrons; therefore, it is employed in nuclear reactors as a material for moderators and reflectors, as well as a coating for fuel elements [1]. The broad application of beryllium is limited, however, due to its high brittleness. The cause of the brittleness of beryllium has not yet been established.

Definite interest is drawn to study of the elastic properties of beryllium, since the magnitude of the modulus of elasticity is characteristic of the interatomic bond in metals and alloys.

EXPERIMENTAL SECTION AND RESULTS

The variation in the dynamic modulus of normal elasticity of beryllium on heating was studied in the present work. The modulus of elasticity was computed from the resonant frequency of the bending vibrations of a freely suspended cylindrical specimen. The measurements were conducted in a vacuum of 10^{-4} mm Hg on the apparatus described in [2]. The specimens took the form of a cylinder 5 mm in diameter and

100 mm in length, which was bored from beryllium bars produced by me-
thods of powder metallurgy. Metal with a 99.8% purity was used.

The resonant frequencies and values of the modulus of elasticity
of beryllium at room temperature are given in Table 1.

The average modulus of elasticity obtained for three specimens at
room temperature was $28,500 \pm 500$ kg/mm^2; this agrees with the litera-
ture data [3].

TABLE 1
Resonant Frequencies and Moduli of Elas-
ticity for Different Beryllium Specimens

1 Номер образца	2 Резонансная частота, гц	3 Модуль упругости, кг/мм²
1	5700	28 500
2	5000	28 800
3	4500	28 600

1) Specimen No.; 2) resonant frequency,
cps; 3) modulus of elasticity, kg/mm^2.

The variation in the modulus of elasticity of beryllium on heat-
ing is shown in Fig. 1. Data from the work [3] (the dotted line) are
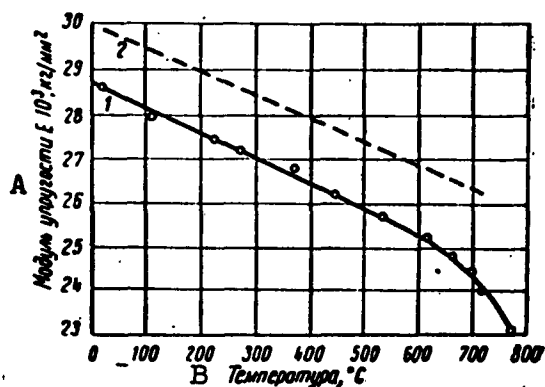also shown here. It is apparent from the diagram that the variation in

Fig. 1. Dependence of modulus of
elasticity of beryllium upon
temperature. 1) Based on our re-
sults; 2) based on data of work
[3]. A) Modulus of elasticity E·
·10^3, kg/mm^2; B) temperature, °C.

- 39 -

the modulus of elasticity is linear in character to a temperature of 600°C. The temperature coefficient of modulus of elasticity in the temperature range from 20 to 600°C is 5.6 kg/mm² per 1°C.

TABLE 2

Temperature Coefficients of Modulus of Elasticity for Certain Metals

1)Металл	Be	2)X18H9T	Ti	Zr
3) Температурный коэффициент модуля упругости в интервале 20--600° C, кг/мм² на 1°C . .	5,6	6,8	6,2	5,1

1) Metal; 2) Kh18N9T; 3) temperature coefficient of modulus of elasticity in range from 20 to 600°C, kg/mm² per 1°C.
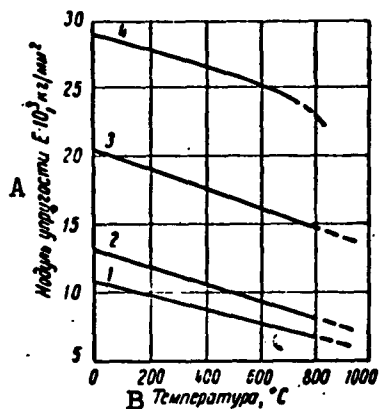

Fig. 2. Dependence of modulus of elasticity of certain metals upon temperature. 1) Zirconium; 2) titanium; 3) Kh18N9T steel; 4) beryllium. A) Modulus of elasticity E· ·10³, kg/mm²; B) temperature, °C.

The difference in the modulus of elasticity as compared with the data of the work [3] can apparently be explained by the difference in the methods of preparing the specimens. The purity, as well as the extent of anisotropy of the metal — factors which exert a noticeable influence on the modulus of elasticity of beryllium — are dependent upon the method of specimen preparation.

Beginning at 600°C, a more rapid reduction was observed in the modulus of elasticity of beryllium. The temperature coefficient of the modulus of elasticity, which was computed in the range from 600 to 750°C, was 13.5 kg/mm² per 1°C.

However, the magnitude of the modulus of elasticity of beryllium was still very high in the temperature range from 600 to 750°C. For comparison, we measured the moduli of elasticity of zirconium, titan-

ium and Kh18N9T steel on the same apparatus.

The results of the measurements are shown in Fig. 2. It is apparent from analysis of the results that although the temperature coefficients of the moduli of elasticity of these metals differ very little from one another (Table 2), the modulus of elasticity of beryllium is considerably higher with respect to magnitude. For example, at a temperature of 600°C, it is triple that of zirconium and is greater than that of Kh18N9T steel by a factor of 1.5.

This large magnitude of the modulus of elasticity of beryllium at both room and elevated temperatures, which is indicative of high inter-atomic-bond strength, is in agreement with the extremely small atomic diameter of beryllium [4].

CONCLUSIONS

1. The modulus of normal elasticity of beryllium was measured on heating to a temperature of 800°C.

2. It was established that the variation in the modulus of elasticity of beryllium is linear to a temperature of 600°C. A more rapid decrease in the modulus of elasticity is observed above this temperature.

3. At elevated temperatures, beryllium has a considerably higher modulus of elasticity than zirconium or titanium. The advantage of beryllium at elevated temperatures is still more obvious if we compare the physical properties referred to unit weight.

REFERENCES

1. Engineer, 209, No. 5431 (1960).

2. Bychkov, Yu.F., Rozanov, A.N. and Skorov, D.M., Atomnaya energiya [Atomic Energy], II, No. 2 (1957).

3. Biver, V. and Uikl', K., Sb.: Berilliy [Collection entitled

Beryllium], No. 4, Moscow, Izd-vo inostr. lit. [Foreign Litera-
ture Publishing House], 1956.

4. Hume-Rothery and Reynor, G.V., Struktura metallov i splavov
    [Structure of Metals and Alloys], Moscow, Metallurgizdat, 1959.

DIFFUSION MOBILITY OF LITHIUM IN IRON AND STEELS*

N.M. Beskorovayniy, V.S. Yeremeyev and

Yu.Ya. Tomasshpolskiy

The liquid metals — sodium, lithium, the lead-bismuth eutectic and others employed as heat-transfer agents in nuclear power engineering — vigorously attack the structural materials at high temperatures. Surface changes occur in the structure of metals [1, 2], mechanical properties are impaired [3] and the thermophysical and other properties are changed. All these changes, which are incorporated in the general concept of corrosion in liquid metals, take extremely diverse forms. Lithium is one of the most aggressive alkali metals as regards corrosion. This may be associated with the diffusion penetration of lithium into the interior of the structural materials, since the presence of lithium in specimens after heating in a molten-metal bath has been established [3].

Diffusion processes have been widely studied with the use of radioactive isotopes. Lithium, however, has short-lived artificially radioactive isotopes (Li^8 with $T_{1/2}$ = 0.9 sec, and Li^9 with $T_{1/2}$ = 0.2 sec); this makes it difficult to use them for study of the diffusion processes.

In the present work, we applied the method of "flame photometry" [4] to determine the lithium concentration in technical iron and carbon steels. This method is a further development of the spectral methods using a photoelement and galvanometer for recording the radiation of a certain substance in place of the usually applied photo-

graphic plate; this enables us to determine small impurities of alkali metals, and lithium in particular with high accuracy.

The alkali metals have a readily excitable spectrum. For lithium in a combustible acetylene-air mixture, it is most convenient to make quantitative analysis on the 6708 A line with an excitation potential of 1.9 ev.
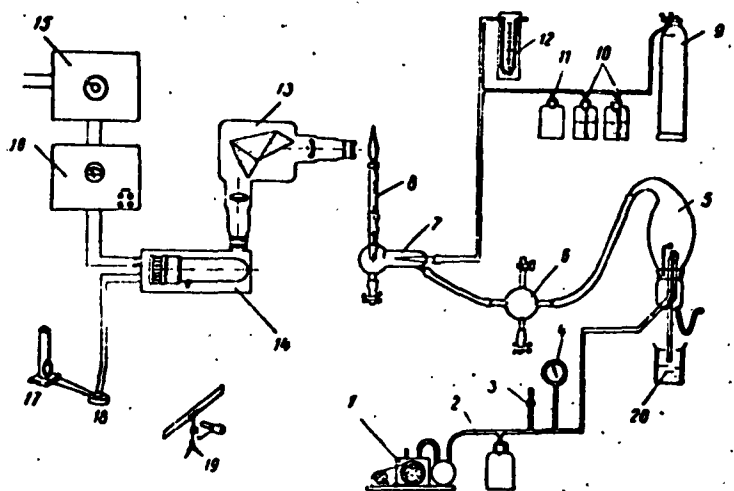

Fig. 1. Scheme of apparatus used for photometry of lithium radiation in flame.

The radiation intensity should be directly proportional to the concentration of the element being determined in solution. A rectilinear relationship was observed for lithium with concentrations to

5γ $(1 \gamma = 10^{-4}$ % by weight of lithium).

Figure 1 shows a diagram of the apparatus for photometry of the emission of lithium in the flame. The solution 20 in which the lithium content is to be determined is transformed into a minute aerosol suspension by the atomizer 5 and fed in such a form into the mixer 7 and then to the burner 8. Large aerosols and drops are caught in the trap 6. Atomization is by compressed air obtained from the compressor 1. Fluctuations in the air pressure are dampened by the ballast volume 2, while the optimum pressure, generally in the range from 0.8 to 1.0 atm,

is set by the tap 3 with reference to the manometer 4. The acetylene
in the cylinder 9, which passes through a purification system 10 con-
sisting of a vessel with a 25% solution of sulfuric acid and a vessel

Fig. 2. Distribution of lithium in
surface layers of Fe, steel 20 and
steel 45 after holding in lithium
at temperature of 600°C. 1) Lithium
concentration, % by weight; 2)
depth of lithium penetration, mm.
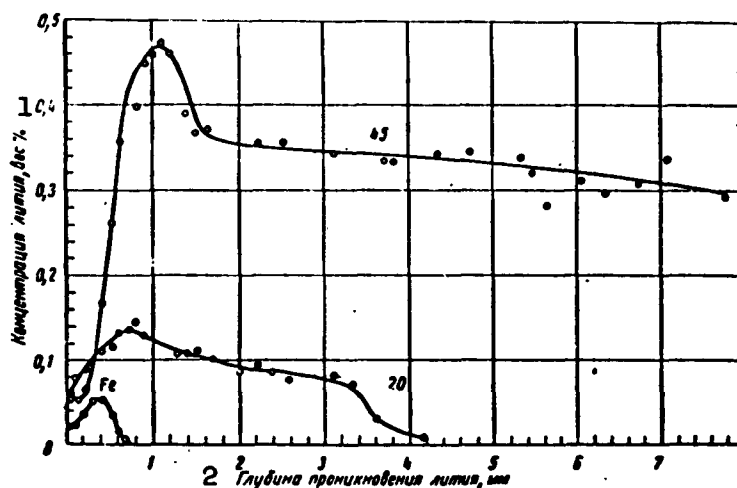
Fig. 3. Distribution of lithium in surface
layers of Fe, steel 20 and steel 45 after
holding in lithium at temperature of 800°C.
1) Lithium concentration, % by weight; 2)
depth of lithium penetration, mm.

with a saturated alcohol solution of iodine, is used as the combustible

gas. The ballast volume 11 assists in maintaining a constant acetylene pressure (12 is a water manometer).

In the mixer 7, the compressed air which is saturated with the aerosols of the solution being investigated, is mixed with the acetylene and the mixture flows into the burner 8.
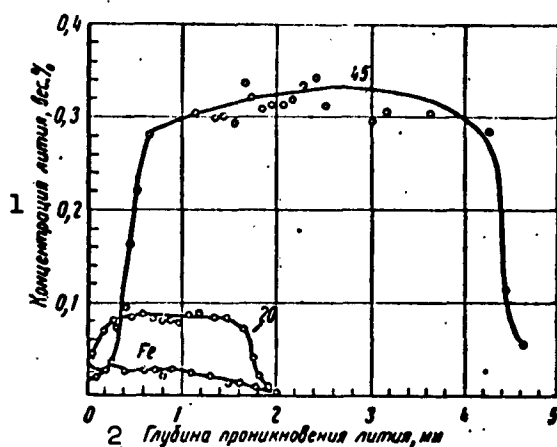

Fig. 4. Distribution of lithium in surface layers of Fe, steel 20 and steel 45 after holding in lithium at temperature of 1000°C. 1) Lithium concentration, % by weight; 2) depth of lithium penetration, mm.
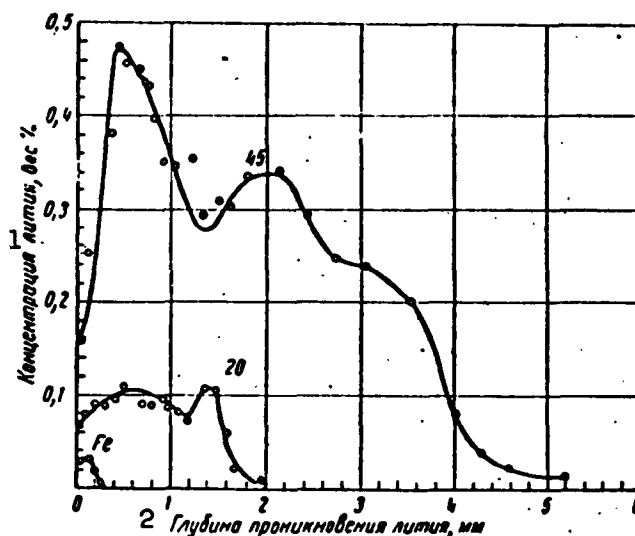
The monochromator 13 (UM-2) emits a line with a wavelength of 6708 A. Its intensity is measured by the photoelectric multiplier 14 (FEU-17) and a galvanometer 17 with a sensitivity of 10^{-8}-10^{-9} amp/mm (18 is a shunt used to vary the sensitivity of the galvanometer). The deflection of the galvanometer's mirror is found from the scale 19.

The photoelectric multiplier is powered by an "Orekh" ["Walnut"] set consisting of the alternating-voltage stabilitron 15 and the high-voltage rectifier 16.

The relative error in determining the lithium content with a large quantity of iron present in solution was not greater than 7%. The lithium concentration was determined by the additives method [4].

The diffusion mobility of lithium in technical iron and carbon steels was determined on cylindrical specimens 12-16 mm in diameter and 30-35 mm in height. The annealed specimens were placed in cups made from commercial iron, filled with lithium in a vacuum apparatus, and the cups were placed in containers made from stainless steel and the lat-
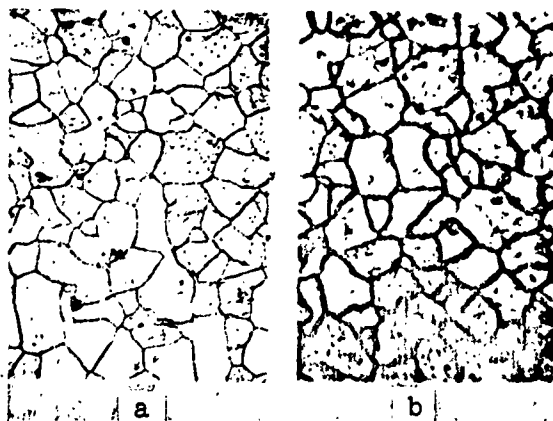

Fig. 5. Microstructure of technical iron. a) Initial state; b) etching of ferrite grain boundaries on polished surface of specimen after holding in lithium at temperature of 800°C for 300 hours (200 x).

ter sealed in an arc furnace in an argon atmosphere. The containers were held at temperatures of 600, 800 and 1000°C. After diffusion holding, the lithium was leached with water. Subsequently, layers 0.05-0.1 mm in thickness were removed from the cylindrical surface of the specimens. The layers were dissolved in a mixture of nitric and hydrochloric acid and, after dilution with water to a certain concentration, the solution was photometered to determine the lithium concentration. By removing sufficiently deep layers from the surfaces, we eliminated the influence of the diffusion of lithium from the faces of the specimens.

Figures 2-4 show the lithium distribution in the surface layers of commercial iron after 25-hour diffusion holding, as well as the dis-

- 46 -

tribution in the surface layers of steel 20 and steel 45 after 3-hour diffusion holding at temperatures of 600, 800 and 1000°C.

All the curves have a maximum regardless of the diffusion holding temperature, and there is less lithium in the surface layers than in the internal layers; the maximum lithium content increases with increasing carbon content in the steel and reaches a significant magnitude — 0.47% — in steel 45. An increase in temperature increases the maximum lithium concentration noticeably only on transition from 600 to 800°C. The depth of the diffusive penetration of lithium also increases with increasing carbon content. The greatest depth of lithium penetration in iron was

Fig. 6. Polished surface of steel 45 specimen after holding in lithium at temperature of 950°C for 4 hours. Surface decarbonized — ferrite. Together with corroded grain boundaries (obviously, former austenitic grains), normal ferrite grain boundaries are observed (600 x).

TABLE 1

Order of Magnitude of Levels of Diffusion Mobility of Lithium from the Formula D = $= \overline{x}^2/2\tau$

1 Материал	2 Коэффициент диффузии лития D, см²/сек при температуре, °C		
	600	800	1000
Техническое железо 3	10^{-8}	10^{-8}	10^{-8}
Сталь 20 4	10^{-7}	10^{-8}	10^{-7}
Сталь 45 5	10^{-8}	$>10^{-8}$	10^{-8}

1) Material; 2) diffusion coefficient of lithium D, cm²/sec at temperature, °C; 3) technical iron; 4) steel 20; 5) steel 45.

observed at a temperature of 600°C and in steel 20 and steel 45 at a temperature of 800°C.

The grain boundaries on the surfaces of the specimens which were held in lithium underwent particularly significant breakdown (Figs. 5, 6); lithium is, so to speak, an etching agent that exposes structure as a result of significant corrosion of the grain boundaries. Obviously, the reduced lithium concentration on the surfaces of the specimens as compared with the internal layers is also explained by this fact, since partial leaching of the lithium along the grain boundaries is possible only after prolonged treatment of the specimens with water.
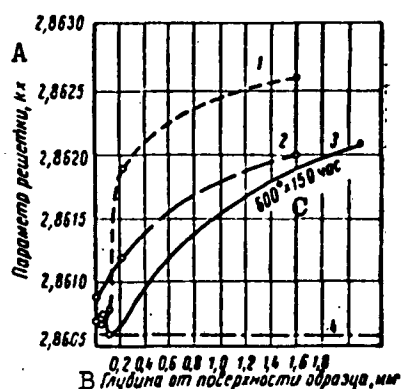

Fig. 7. Variation in parameters of crystal lattice of commercial iron after holding in lithium. 1) At 1000°C for 150 hours; 2) at 800°C for 300 hours; 3) at 600°C for 150 hours; 4) tabular data for pure iron. A) Lattice parameter, kX; B) distance from surface of specimen, mm; C) 600° x 150 hours.

From the depth of lithium penetration in iron and steel, it is possible to evaluate the diffusion coefficient of lithium approximately by the formula

$$D = \frac{\bar{x}^2}{2\tau}.$$

where D is the diffusion coefficient in cm^2/sec, $\bar{x}$ is the average depth of penetration of the diffusing element in cm and τ is the time of diffusion holding in sec.

The formula in question is correct for cases of bulk diffusion. However, with a certain approximation, this formula may give an idea of the order of magnitude of the level of diffusion mobility of lithium.

Evaluation of the diffusion mobility of lithium from the above formula is probably less correct for commercial iron, since the grain boundaries in the surface layer undergo considerable thickening (visible corrosion effect) after diffusion holding in lithium, and it is possible that in commercial iron, the diffusion of lithium proceeds

mainly through the grain boundaries.

Table 1 gives the order of magnitude of the levels of the diffu-
sion mobility of lithium as computed from the above formula.

TABLE 2

Data on Microhardness of Ferrite in Steel 20
and Steel 45

1 Материал	Температура выдержки в литии, °C 2	Время выдержки, 3	4 Микротвердость, H_V, кг/мм²		
			5 в поверхностных слоях	6 в более глубоких слоях	7 исходное состояние
8 сталь 20	800	3	103—114	133—154	174—178
9 сталь 45	600	3	109—114	174—199	—

1) Material; 2) holding temperature in lithi-
um, °C; 3) holding time, hours; 4) microhard-
ness, H_V, kg/mm²; 5) in surface layers; 6) in
internal layers; 7) initial state; 8) steel
20; 9) steel 45.
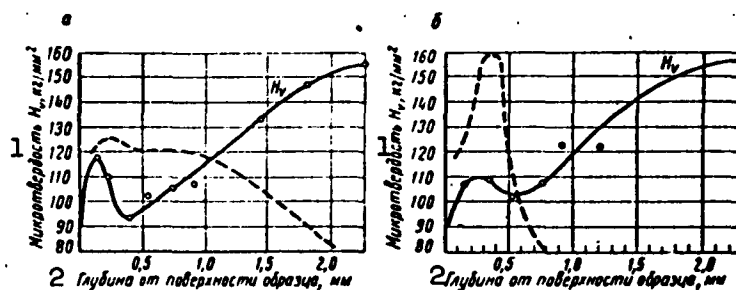
Fig. 8. Variation in microhardness of surface
layers of commercial iron after 100-hour hold-
ing in lithium at temperature of 600°C (a)
and 800°C (b) (concentration curve of lithium
distribution is indicated by broken line). 1)
Microhardness H_V, kg/mm²; 2) distance from
surface of specimen, mm.

The data given in Table 1 attest to the high diffusion mobility
of lithium in steels, which is comparable in order of magnitude to the
diffusion mobility of carbon. Carbon increases the penetration depth
of lithium. The diffusion mobility of lithium was lower in γ-iron than
in α-iron.

The influence of carbon is detected both at a temperature of 600°C, when it is present in steel in the form of Fe_3C, and at temperatures of 800 and 1000°C when it was present in the form of a solid solution in γ-iron. Obviously, when lithium diffuses, we obtain considerable development in the reactive-diffusion process, because the lithium possesses a high chemical affinity to carbon, forming a lithium carbide Li_2C_2 with a density of 1.65 g/cm³ [5]; according to the diagram of state of $Li-Li_2C_2$ [6], a low-melting eutectic forms with lithium ($t_{pl} \approx 165°C$) at approximately 1 atom-% of carbon.

Lithium that has diffused into iron and steel exerts a refining influence, reducing the impurity content in the ferrite grains, as well as in the steel as a whole. Thus, x-ray examinations show that after holding in lithium, the crystal-lattice parameters in the surface layer of commercial iron decrease to values close to the crystal-lattice parameters of pure iron (Fig. 7).

In carbon steels, the carbon content decreases sharply in the surface layers.

Surface layers of commercial iron that have been subjected to the corrosive action of lithium have a lower microhardness (Fig. 8).

The microhardness of ferrite is also reduced in the carbon steels (Table 2).

A reduction in microhardness is possible, however, not only where the concentration of the dissolved impurities decreases, but also where microscopic pores and sponginess form in the surface layer. Obviously, the formation process of the microscopic pores and porous properties does not play the least significant role in the corrosive action of liquid lithium.

Data on the diffusion mobility of lithium in iron and steel show that significant changes in structure as well as in properties for

example, microhardness, is observed only in a layer into which the lithium has diffused. In the surface layer of commercial iron, the corrosive action of lithium appears mainly along the grain boundaries.

The grain boundaries have the greatest number of defective zones, which facilitate the diffusion process, and, in addition to this, accumulation of impurities (for example, carbon, sulfur and others) with which lithium vigorously enters into reaction is possible at the boundaries.

Fig. 9. Microstructure of surface layer of commercial iron after holding in lithium at temperature of 600°C for 200 hours. Development of corrosion along ferrite-grain boundaries (600 x).

Figure 9 shows the microstructure of the surface layer of commercial iron after holding in lithium at a temperature of 600°C over a period of 200 hours. The corrosive action of the lithium is manifested in a considerable thickening of the grain boundaries. This is possibly the result of a reaction between the lithium and tertiary cementite, segregations of which were observed on prolonged holding in the layers where lithium was absent.

According to the diagram of state of $Fe-Fe_3C$, the appearance of an austenite network with a carbon content of approximately 0.5-0.7% is possible along the grain boundaries of commercial iron on heating to 800°C. The change in the structure of commercial iron in a medium of liquid lithium at a temperature of 800°C also occurs basically along the grain boundaries, but the nature of the corrosion breakdown changes somewhat and the diffusion mobility of the lithium is reduced (Figs. 10, 11).

Fig. 10. Microstructure of surface layer of commercial iron after holding in lithium at temperature of 800°C for 200 hours. Formation of new phase along ferrite grain boundaries, as well as development of phases nonhomogeneous with respect to shape and size of ferrite grains (600 x).
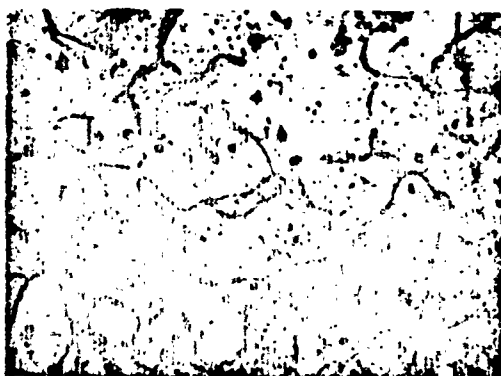

Fig. 11. Same as in Fig. 10. Corrosive action of lithium along grain boundaries, as well as partial corrosion in grains themselves (600 x).

At temperatures over 910°C, iron enters the state of the γ-phase, in which the carbon impurities present in technical iron (0.03-0.06%) are dissolved.

The diffusion of lithium is made even more difficult; possibly, this is linked with the reduced impurity content along the grain boundaries.

Generally, the austenitic grain in commercial iron grows rapidly at high temperatures; however, in a layer where lithium has diffused, the grain growth is almost completely arrested, since products of corrosion or phases rich in lithium, which inhibit grain growth, form along the grain boundaries (Fig. 12). The increase in grain size becomes noticeable only on prolonged holding, for example, for 100 hours at a temperature of 1000°C.

A new form of corrosion breakdown — a network of points, which does not coincide with the ferrite grain boundaries — also appears where lithium is present in the surface layers of commercial iron at temperatures of 800-1000°C (Fig. 13). The most likely reason for the reticular corrosive action of lithium at temperatures of 800-1000°C is

Fig. 12. Microstructure of commercial
iron after heating at temperature of
1000°C for 50 hours. a) Heated in ar-
gon atmosphere, large ferrite grains;
b) heated in medium of liquid lith-
ium, relatively small ferrite grains,
along whose are indications of corro-
sive action of lithium (200 x).

Fig. 13. Microstructure of commer-
cial iron. a) Unetched microsection
of surface layer after heating in
lithium at temperature of 800°C
for 250 hours. Corrosion breakdown
in form of network of points
(300 x); b) same, after annealing
at temperature of 920°C for 1 hour;
traces of corrosion breakdown are
retained in form of network (200 x).

sulfur impurities along the boundaries of the former austenitic grains. Figure 14 depicts a radioautogram of the sulfur distribution in commercial iron after extremely slow cooling from the liquid state. Some of
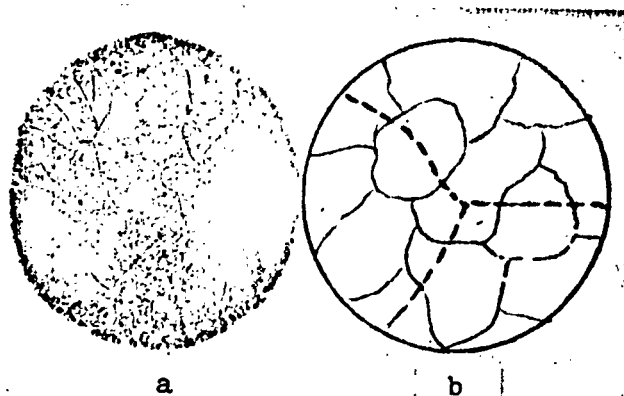

Fig. 14. Radioautogram of sulfur distribution in commercial iron after extremely slow cooling from liquid state (a) and scheme of reticular sulfur distribution (b).

the sulfur is in solid solution in the ferrite, as is attested to by the uniform blackening of the entire field of the radioautogram; some of the sulfur is distributed in the form of a network of points, as well as in the form of a fine-meshed, almost continuous network; here the two forms of reticular sulfur distribution are not linked with one another.

In commercial iron, sulfur may be present in the form of the compound FeS, which forms a low-melting eutectic $(t_{pl} = 985^{\circ}C)$ with iron.
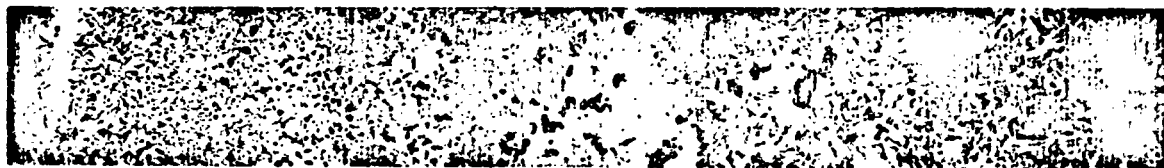

Fig. 15. Microstructure of surface layer of steel 70 after holding in lithium at temperature of 800°C for 3 hours. Surface layer is decarbonized: black inclusions appear instead of perlite; initial structure is in internal layers.

The FeS-Fe eutectic is precipitated along the grain boundaries on extremely slow cooling and the eutectic sulfur is fixed in the form of a network of points on the radioautogram. On subsequent transformation of the γ-iron into α-iron ($t_{prevr} = 910^{\circ}C$), part of the sulfur dissolved in the γ-iron precipitates out along the grain boundaries of the new ferrite grains in the form of a fine-meshed, almost continuous network, since the solubility of the sulfur is somewhat lower in the α-iron.

In commercial iron, therefore, we observe a complete analogy between the nature of the sulfur distribution and that of the corrosive breakdown in a medium of liquid lithium in the form of a network of points. This again confirms the data of [1], where it was shown that sulfur inclusions may act as seats of corrosion breakdown.

In a medium of liquid lithium, the structure of the carbon steels changes to an even more significant degree. In the surface layer, lithium breaks up cementite at a temperature of $600^{\circ}C$, while it attacks a carbon austenite at $800-1000^{\circ}C$; carbon is leached out. The structural component of perlite disappears in the surface layer and black inclusions — a product of the corrosive action of the lithium — appear. This is seen most clearly on a sample of steel 70, which was held in lithium at a temperature of $800^{\circ}C$ over a period of 3 hours (Fig. 15).

Under the corrosive action of lithium, the thickness of the decarbonized layer increases with increasing carbon content, as well as at increased holding temperatures (Fig. 16).

Data on the distribution of lithium show that the depth of lithium diffusion is approximately double that of the breakdown observed in the structure.

Thus, in carbon steels (as in iron), the corrosion breakdown of the structure occurs only in volumes that are saturated with diffused

TABLE 3

Mechanical Properties of Carbon Steels After Holding in Argon and Lithium

1 Марка стали	2 Температура выдержки, °C	3 Время выдержки, ки. ч	4 σ_b, кг/мм²		δ, %	
			5 выдержка в аргоне	6 выдержка в литии	5 выдержка в аргоне	6 выдержка в литии
7 Сталь 20	600	50	41,8	35,3	32,8	30,2
	800	50	48,6	31,7	29,4	12,0
	1000	50	43,3	22,5	33,9	10,0
8 Сталь 45	600	50	56,7	27,6	25,0	21,5
	800	50	66,0	16,4	22,0	2,9
	1000	50	76,2	14,2	15,0	1,4
9 Сталь 70	600	50	63	12,9	22,0	4,1
	800	50	84,5	9,9	10,9	1,9
	1000	50	104	5,5	6,5	1,0

Note: Cooled in air after holding in argon and lithium.

1) Type of metal; 2) holding temperature, °C; 3) holding time, hours; 4) σ_b, kg/cm²; 5) holding in argon; 6) holding in lithium; 7) steel 20; 8) steel 45; 9) steel 70.

lithium; here the breakdown of the structure obviously occurs only after accumulation of a sufficient quantity of lithium, since the depth of diffusive penetration of the lithium exceeds that of the structural breakdown.

Considerable volume changes occur in carbon steels that are held in a medium of liquid lithium; the dimensions of the specimens increase and the density of the carbon steels decreases, and the more so the higher the carbon content in the steel (Fig. 17).

The increase in the dimensions of the specimens and the decrease in the density of the carbon steels after holding in lithium are possible only on formation of phases with low density, for example, lithium carbide, which has a density of 1.65 g/cm³, or other phases. This fact is once again indicative of the major role played by the physicochemical processes on volume diffusion of lithium in steels and commer-
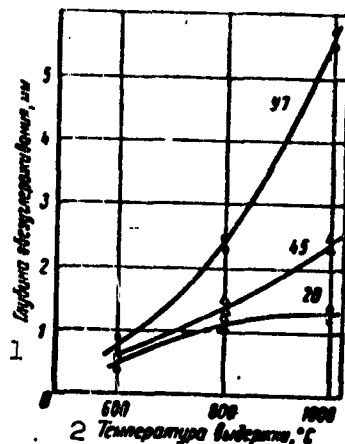
Fig. 16. Depth of de-
carbonization in car-
bon steels after
holding in lithium
for 3 hours, as ob-
served on microscopic
investigation. 1)
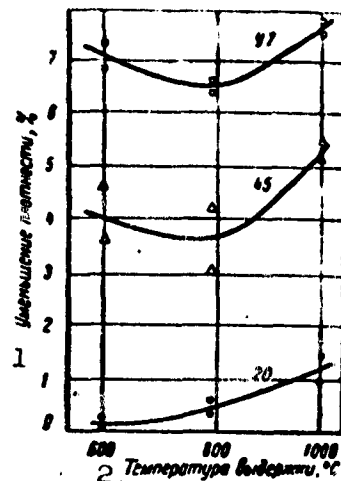Depth of decarboniza-
tion, mm; 2) holding
temperature, °C.

Fig. 17. Variation in
density of carbon
steel specimens after
holding in lithium
for 3 hours. 1) Reduc-
tion in plasticity,
%. 2) holding tempera-
ture, °C.

cial iron. The formation of low-density phases at high temperatures
is accompanied by significant plastic deformation as a result of which
cracks form on cooling (Fig. 18).

Fig. 18. Cracking on steel
70 specimens after holding
in lithium for 50 hours at
temperatures of 600°C (a),
800°C (b) and 1000°C (c).

The change in structure caused by
the diffusive penetration of lithium
into iron and carbon steels is accom-
panied by changes in many properties. As
has already been noted, the microhard-
ness of the surface layers is reduced
and the density decreases. In addition
to this, the mechanical properties of
the carbon steels change sharply: the

strength and plasticity are reduced (Table 3).

The reduction in mechanical properties proceeds quite vigorously

in steels with high carbon contents and at higher temperatures. Thus, steel 45 and steel 70 acquire the properties of low-quality cast iron at holding temperatures of 800-1000°C. Such sharp embrittlement of the steels and the decrease in density may be explained only by the presence of a large number of micropores, as well as a significant quantity of low-strength phases formed as a result of diffusion of lithium and subsequent breakdown of the structure.

CONCLUSIONS

1. Lithium has considerable diffusion mobility in commercial iron. Its penetration increases sharply in carbon steels due to the presence of carbon.

2. The changes in the structures of commercial iron and carbon steels are linked with the diffusive penetration of lithium; they occur only in those volumes where there is a sufficient quantity of lithium as a result of diffusion.

3. The penetration of lithium occurs principally through the grain boundaries which are usually rich in impurities: carbon, sulfur and others.

4. Lithium exerts a refining influence in regard to carbon and other admixtures in commercial iron and carbon steels.

5. The changes in the structures of commercial iron and carbon steels as a result of diffusion of lithium lead to a decrease in density, the appearance of micro- and macrocracks, significant reduction in strength and embrittlement of the carbon steels.

Manu-script Page No.	[Footnote]
42	Ye. A. Korepanov, L. M. Ozerov and M. V. Teregulov participated in the work.

REFERENCES

1. Beskorovanyy, N.M. and Yakovlev, Ye.I., Sb. Metallurgiya i metallovedeniye chistykh metallov [Metallurgy and Physical Metallurgy of Pure Metals], No. II, Moscow, Atomizdat, 1960.

2. Brasunas. Corrosion, 9, No. 3, 78-84 (1953).

3. Lyashenko, V.S., Zotov, V.V. Andreyev, V.Ye., Abramovich, M.D. and Ivanov, V.A., Tr. Vtoroy mezhdunarodnoy konferentsii po mirnomu ispol'zovaniyu atomnoy energii (Zheneva, 1958). Dokl. sovetskikh uchenykh. [Trans. of the Second International Conference on the Peaceful Uses of Atomic Energy (Geneva, 1958). Reports of Soviet Scientists], Vol. 3, Moscow, Atomizdat, 1958.

4. Poluektov, N.S., Metody analiza po fotometrii plameni [Methods of Analysis in Flame Photometry] Moscow, Goskhimizdat [State Scientific and Technical Publishing House for Chemical Literature], 1959.

5. Slavinskiy, M.P., Fiziko-khimicheskiye svoystva elementov [Physicochemical Properties of Elements], Moscow, Metallurgizdat, 1952.

6. Fedorov, I.P. and Su Myan' Tszen, Khusyue Cyuebao, 23, No. 1 (1957).

THE SOLUBILITY OF METALS IN CARBON

Yu.G. Godin, A.I. Yevstyukhin, V.S. Yemelyanov,

A.A. Rusakov and I.I. Suchkov

Vast theoretical and practical interest is drawn to investigation of the solubility of metals in carbon. Thus far, however, there is no reliable information as regards this problem in the literature sources. To all appearances, this problem is linked with a number of specific difficulties consisting basically in the complexity of introducing small quantities of metallic additives into carbon and uniform distribution of them throughout the volume of the specimen. These difficulties are due to the high melting points of carbon, which exceed $4000^{\circ}C$, and its vapor pressure, which goes beyond 100 atm at the melting point.

As a result of the above, it has not been possible to prepare carbon specimens for solubility investigation by the usual methods (by melting the components, powder metallurgy and diffusion).

In order to facilitate solution of the problem relating to the solubility of metals in carbon, the authors divided it into two stages. The problem of the first stage was to determine the presence or absence of solubility; in the second stage, it was proposed to establish the magnitude of the maximum solubility in cases where it occurs. The present paper describes the results of the first stage, which were achieved with zirconium and niobium.

For solution of the problem concerning the presence or absence of solubility, we proceeded from the following. In the case of solubility of one component in another, when an alloy which lies in the hetero-

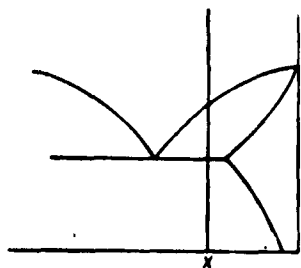geneous region (for example, alloy x in Fig. 1) is hardened from the solidus temperature, the quantity of the dissolved component should correspond to its maximum content in the crystals of the dissolved component. In conformity with the segment rule. Removing the crystals from the basic mass of the specimen and studying them, we may establish the presence or absence of solubility and determine its magnitude.

Fig. 1. Part of diagram of state of eutectic type with limited solubility.

On studying the diagrams of state of the zirconium-carbon and niobium-carbon systems, we established that preparation of alloys of these systems is possible by melting in an

Fig. 2. Microstructure of cast hypereutectic alloy of zirconium-carbon system. Primary grains are of carbon and eutectic consisting of carbon and carbide (200 x).

arc only up to certain carbon concentrations in view of its high volatility at high temperatures. Study of the microstructure of alloys whose carbon contents lay close to the maximum values indicates the presence in the alloys of "free" graphite, which enters into the eutectic composition and separates out in the form of primary crystals. Microstructures of alloys of the carbon wi n zirconium and niobium that we obtained are shown in Figs. 2 and 3. These alloys consist of

primary graphite grains and a eutectic — a mixture of graphite and the carbides of zirconium or niobium, respectively.

Alloys of carbon with zirconium and niobium were smelted in an MIFI-9-3 arc furnace with a cooled copper sole in an atmosphere of argon. When the alloys were prepared, a graphite tip with a high degree of purity was used in place of a tungsten tip. This replacement was made in order to decrease the volatility of carbon from the alloy specimens and to eliminate tungsten contamination of the alloys. Spectrally pure carbon sticks, 99.8% pure iodide zirconium rods and 99.3% pure fragments of rod niobium were employed as starting materials. A mixture consisting of carbon and metal fragment was melted several times in the arc furnace in order to obtain uniform distribution of the components. The magnitude of the arc current was established in such a manner that the alloy being melted formed a liquid drop.
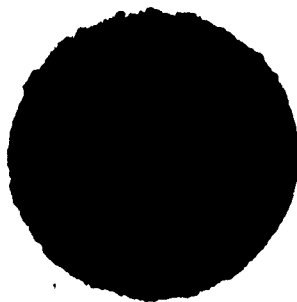

Fig. 3. Microstructure of cast hypereutectic alloy of niobium-carbon system. Primary grains are of carbon and eutectic consisting of carbon and carbide (200 x).

Since cooling of the alloys occurred very rapidly on the copper sole in the arc furnace, it is obvious that the prepared alloys were hardened from temperatures lying about the solidus line. To determine the solubility of the zirconium and niobium, it was necessary to separate the carbon from the carbide mass. The separation was carried out by two methods: by separating the carbon and carbides in a gravity solution and by chemically dissolving the carbides. To separate the carbon in the carbides by the former method, the alloys were transformed into a fine powder which passed through a 270-mesh screen. The screened powder fraction was poured into a test tube with bromoform (density 2.8-2.9 g/cm^3),

which was placed in a centrifuge. After centrifuging, a small quantity of the powder remained on the surface of the bromoform; this was filtered through filter paper and washed free of bromoform with alcohol. In addition to graphite lines, we also observed carbide lines on radiograms obtained from exposure of this powder; this was indicative of incomplete separation of the carbon and carbides. It is quite possible that this separation procedure would be found more satisfactory if the alloys were ground finer.

Application of the latter method, chemical solution, enabled us to produced a graphite free from carbides. This method consisted in the following: a finely ground alloy powder was passed through a 270-mesh screen and dissolved by heating in a platinum dish in a mixture of hydrofluoric and nitric acids. Here the carbides were dissolved, while the graphite was found to be in the undissolved residue. After the powder was carefully washed and dried, the graphite was subjected to x-ray analysis. A similar analysis of spectrally pure carbon was made for comparison.

Radiograms of the specimens were produced in a cylindrical RKU-86 chamber with filtered CuK_α-radiation. The exposure was made with the sharp-focus tube at a voltage of 45 kv and current of 2 ma over a period of 2 hours. The specimens used for exposure were prepared by packing the powders into celluloid capillaries.

A radiogram obtained on the graphite which had been separated from zirconium carbide is shown in Fig. 4. A similar radiogram was taken on graphite which had been separated from niobium carbide. A radiogram of spectrally pure carbon is shown in Fig. 5. On the latter radiogram, the lines with large glancing angles were blurred; this is apparently linked with the small particle sizes of the investigated specimen. The doublet splitting of the rear lines is clearly apparent

Fig. 4. Radiogram of graphite separated from zirconium carbide.

on the radiogram shown in Fig. 4. The values of the distances between planes as were determined from the radiogram were compared with data on Ceylon graphite [1] and the values computed from the work [2]. The

Fig. 5. Radiogram of spectrally pure carbon.

results of the comparison are shown in the table.

It is apparent from Figs. 4 and 5 and the data in the table that there is splitting of the 004 line on the radiogram of the spectrally pure carbon, and the 006 line on the radiogram of the graphite sepa-

Comparative Values of Distances Between Planes
in Different Graphite Specimens, A

hkl	1 d, рассчитанное по [2]	2 d цейлонского графита [1]	3 d спектрально чистого угля	4 d графита, отделенного от карбида
002	3,347	3,35	3,41	3,35
010	2,127	2,14	2,12	2,12
011	0,027	2,04	2,02	2,03
012	1,795	1,80		1,79
001 *	1,673	1,67	1,685 / 1,661	1,682 / 1,655
013	1,510	1,54		1,536
014	1,315	1,32		
110	1,229	1,23	1,226	1,226
112	1,152	1,15	1,151	1,150
015	1,133	1,13		
006 *	1,116	1,11	1,116	1,116 / 1,112
021	1,05	1,05	1,047	1,046
016	0,9881		0,9864	0,987
008	0,8370		0,8368	0,9369
116	0,8260		0,8251	0,8252
120	0,8040			0,8055
121	0,7984			0,7992

*The lines were separated.

1) d, computed from [2]; 2) d of Ceylon graphite [1]; 3) d of spectrally pure carbon; 4) d of graphite separated from carbide.

- 64 -

rated from the zirconium carbide. This splitting cannot be explained
by the presence of graphites with two different periods c in the spe-
cimen, since it is apparent from the table that the magnitude of this
splitting decreases with increasing Bragg angle. It is interesting to

3601,193 Å   3547,682 Å   3519,603 Å

Fig. 6. Segments of spectra. 1) Iron; 2)
iodide zirconium; 3) spectrally pure car-
bon; 4) graphite separated from zirconium
carbide.

note that the above splitting was not observed on the radiogram of
Ceylon graphite. Comparison of the distances between the planes for
the graphite that we separated with the corresponding values computed
from the data of [2], shows an agreement within the limits of measure-
ment error. Thus, x-ray examination shows no solubility of niobium and
zirconium in graphite.

To confirm the x-ray data, we conducted a spectral analysis of
the graphite that we obtained, part of whose spectrogram is shown in
Fig. 6. For comparison, the spectrograms of iodide zirconium and the
initial spectrally pure carbons which were used in preparation of the
alloys are shown on the same illustration; the last spectral lines of
the zirconium are indicated by the arrows. Study of these spectra
failed to indicate the presence of zirconium in the graphite which had
been separated from the zirconium carbide. Since the sensitivity of

- 65 -

the zirconium determination by the spectral method is of the order of 0.01%, we may assume that the solubility of zirconium in graphite, if any, is less than 0.01%. Similar results were obtained for the solubility of niobium in carbon.

CONCLUSIONS

1. A method of determining whether a number of high-melting metals are soluble in carbon was proposed.

2. X-ray and spectral examinations did not indicate solubility of zirconium and niobium in carbon.

REFERENCES

1. Zap. Leningr. gornogo in-ta [Notes of the Leningrad Mining Institute], 11, No. 2 (1938). Rentgenograficheskiy opredelitel' mineralov [X-Ray Mineral Determiner], Part 1, p. 65.

2. Nelson, Reley. Proc. Phys. Soc., 57, 477 (1945).

Manu-script Page No.	[List of Transliterated Symbols]
50	пл = pl = plavlyeniye melting
55	превр = prevr = prevrasheniye = transformation
56	в = v = vyderzhka = holding

DISTRIBUTION LIST

DEPARTMENT OF DEFENSE	Nr. Copies	MAJOR AIR COMMANDS	Nr. Copies
		AFSC	
		SCFDD	1
		DDC	25
HEADQUARTERS USAF		TDBTL	5
		TDBDP	5
AFCIN-3D2	1	ASD (ASYIM)	1
ARL (ARB)	1	AEDC (AEY)	1
OTHER AGENCIES			
CIA	1		
NSA	6		
DIA	9		
AID	2		
OTS	2		
AEC	2		
PWS	1		
NASA	1		
ARMY (FSTC)	3		
NAVY	3		
NAFEC	1		
RAND	1		
SPECTRUM	1		
AFCRL (CRXLR)	1		